SUPPLEMENTARY APPENDIX

Timing and cause of mid-Holocene mammoth extinction on St. Paul Island, Alaska

Russell W. Graham, Soumaya Belmecheri, Kyungcheol Choy, Brendan J. Culleton, Lauren J. Davies, Duane Froese, Peter D. Heintzman, Carrie Hritz, Joshua D. Kapp, Lee Newsom, Ruth Rawcliffe, Émilie Saulnier-Talbot, Beth Shapiro, Yue Wang, John W. Williams, Matthew J. Wooller

Table of Contents

Supplementary Text

S1. St. Paul Island size reconstruction

Materials and methods

Dates in the text are reported as y ago and dates in supplementary text are reported as cal. years BP. Both methods are equivalent. The size and area of St. Paul Island from ~14,500 calendar years before present (cal. years BP; present is defined as 1950 CE) (70 m below modern sea level) to recent was reconstructed with geographic information system (GIS) analysis of 70 raster grids (24 × 24 m cells) projected in the Universal Transverse Mercator (Z2N, NAD 1983) co-ordinate system. Seventy grids were generated using a mosaicked bathymetric grid and an ASTER DEM (Advanced Spaceborne Thermal Emission and Reflection radiometer digital elevation model). The bathymetric grid was created using 1:50,000 and 1:200,000 depth charts (NOAA 2006). The soundings were digitized in ArcGIS with fathoms converted to feet during the digitizing process and further converted to meters in the ArcMap table. A triangular irregular network (TIN) was generated from the point data, which was converted to a raster grid matching the cell size and snapped to an available ASTER DEM for St. Paul Island. To generate the individual island area rasters, the DEM was classified to display only the cells for sea levels between 1 and 70 meters below modern sea level. An analysis box was edited to eliminate non-contiguous cells (islands not part of the main St. Paul Island) and to set the analysis extent for generating the 70 rasters. Island area was calculated by multiplying the total number of cells for each sea level by 24 × 24 m. To add a temporal designation to each sea level and island area, we used the predicted relative sea level curve for the Bering Strait (1).

Results

St. Paul Island was part of the Beringian mainland and land bridge at 14,710 cal. years BP, during which sea level was 80 m below that of today (Fig. 1b). At 13,560 cal. years BP, St. Paul became a large island, separate from mainland North America, when sea level was 70 m below modern sea level (Fig. 1b). St. Paul Island continued to shrink as sea level rose and attained its current land area ~6,400 cal. years BP (Figs. 1b, 2).

S2. Radiocarbon dating and isotopic analyses of mammoth remains

Three mammoth tusk and 11 tooth remains found by local residents from St. Paul Island were radiocarbon dated and vouchers are preserved in the Earth and Mineral Sciences Museum at PSU (Table S1). Collagen for accelerator mass spectrometry (AMS) radiocarbon (^{14}C) was extracted and purified using the modified Longin method with ultrafiltration (2). Physically cleaned samples were demineralized and gelatinized in 0.01 N HCl. Crude gelatin yields were recorded and the gelatin was ultrafiltered, retaining >30kDa molecular weight gelatin. Carbon and nitrogen concentrations and stable isotope ratios were measured at the Yale ESCSIS facility with a Costech EA (ECS 4010) and a Thermo DeltaPlus Advantage analyzer. Sample quality was evaluated by % crude gelatin yield, %C, %N, and C:N ratio (3). Samples were processed at the Human Paleoecology and Isotope Geochemistry Laboratory at the Pennsylvania State University (PSU) with AMS ^{14}C dating conducted at the Keck-CCAMS, University of California, Irvine. All AMS ^{14}C results were corrected for isotopic fractionation according to standard conventions (4), and calibrated in OxCal 4.2.3 (5) with the IntCal13 curve (6). All dates in this study are reported as calendar years before the present (cal. years BP; present is defined as 1950 CE).

S3. Lake Hill composite core

Construction and sampling

Three cores within a 3 m lateral distance were extracted from the central part of Lake Hill (57.17809ºN, 170.24828ºW) (Figs. S1, S2) at 1.3 m water depth under a ~30 cm ice layer with a Livingston piston corer. The second and third cores extended ca. 1 m deeper than those from the first core. A composite core and linear master depth scale (Mean Composite Depth; MCD) is constructed by using clearly identifiable marker layers, such as visible tephras and lithologic transitions, to cross-correlate equivalent depths among overlapping sections of the three cores (Fig. S2). We also collected a second set of overlapping cores at a more shoreward location (57.17840ºN, 170.24876ºW) but did not analyze these sediments. All cores have been archived at the National Lacustrine Core Facility (LacCore, University of Minnesota) and are available for further analysis.

The composite record was analyzed for magnetic susceptibility, spectrophotometry and high-resolution digital photography and sampled for a variety of paleoecological and

paleoenvironmental proxies at LacCore. These proxies included tephra, sedimentary ancient DNA (sedaDNA), coprophilous spores, pollen, macrobotanical remains, diatoms, cladocerans, and chironomids, which were sampled at differing resolutions (Table S2).

Age model reconstruction

A Bayesian age model for the upper 740 cm of the composite core (Fig. S3) was constructed from one tephra layer (Section S4) and AMS ^{14}C dating of six opportunistically sampled terrestrial macrobotanical remains, consisting of unidentified dicot leaves or moss gametophores (Table S3). Samples were processed for radiocarbon dating at the Human Paleoecology and Isotope Geochemistry Laboratory at the Pennsylvania State University (PSU) with AMS ^{14}C dating conducted at the Keck-CCAMS, University of California, Irvine. All AMS ^{14}C results were corrected as described above. The age model was generated using a Poisson process deposition model (P-Sequence) in OxCal 4.2.3 calibrated with the IntCal13 curve, assuming a *k* parameter of 0.6, or one event every 1.67 cm, and ages per depth were interpolated to every centimeter. All MCD-derived dates in this study were inferred from this age model.

S4. Tephra analyses

Materials and methods

We identified both visible tephra and non-visible cryptotephra layers from contiguous samples of material between 0-765 cm depth at 2 cm resolution (Table S2). Shard concentration profiles against depth highlight potential peaks of primary air-fall. Glass was re-extracted from these samples for geochemical analysis which is used to correlate tephra with other samples of known age and provenance. Cryptotephra extraction followed standard methods (7), with the exception of substituting the heavy liquid lithium sodium polytungstate for sodium polytungstate. Given the large concentrations of glass present in the samples, *Eucalyptus* pollen was added as a spike when constructing the shard concentration-depth profiles.

Extracted glass samples were mounted within acrylic pucks, polished to expose flat shard surfaces, coated with carbon and then analyzed with a JEOL 8900 superprobe with wavelength dispersive spectrometry (WDS) at the University of Alberta. A standard suite of major elements (Si, Al, Ti, Fe, Ca, Mn, Mg, Na, K, Cl) were targeted using a defocused beam of 10 μm diameter, 15 keV accelerating voltage and 6 nA beam current. Two secondary standards of known composition were run concurrently with all tephra samples: ID3506, a Lipari rhyolitic obsidian, and a reference sample of Old Crow tephra, a well-characterized, secondarily-hydrated tephra bed (8).

To identify potential correlatives, the geochemical data were compared to a database of known eruptions from the published literature. A visible tephra layer at 294cm MCD in the cores correlates with Aniakchak CFE II tephra (Fig. S4, Tables S3, S4). This has a known age of 3,595 ± 4 cal. years BP (9) and the Aniakchak tephra was therefore used as one of the constraints for the age model.

S5. Sedimentary ancient DNA analyses

Overview

Lacustrine deposits have been shown to potentially preserve sedimentary ancient DNA (sedaDNA) (10). Lacustrine sedaDNA can include that derived from the waste (urine, feces) or discarded

tissues (skin, hair, nails) (11, 12) of mammals that lived on or near the lake margin (10, 13). Here, we used sedaDNA preserved in the Lake Hill sedimentary record to examine when mammoths disappeared from the area surrounding the Lake Hill lake on St. Paul Island.

Briefly, we extracted sedaDNA from 38 samples throughout the upper 740 cm (MCD) of the core at the Paleogenomics laboratory, UC Santa Cruz (UCSC) (Fig. S5, Table S5). We converted DNA extracts into libraries, which were Illumina shotgun sequenced. Sequencing reads were merged, complexity filtered, and aligned to the African elephant and woolly mammoth genomes (Table S6). We removed aligned reads that may have had an exogenous, non-mammoth origin. Retained reads were characterized as being consistent with aDNA through the inspection of fragment length distributions, fragmentation patterns, and cytosine deamination rates (Fig. S6). As a negative control to quantify the rate of random read mapping, we also performed these analyses on reads aligned to the two-toed sloth genome.

Materials and methods

*Sample collection***.** To monitor if DNA recovered from inside the drilled cores was introduced by contamination from the drilling procedure or from DNA leaching (14), we sprayed the inside of the Livingston piston coring equipment with American alligator polymerase chain reaction (PCR) amplicons prior to core drilling. These amplicons consisted of five PCR products that ranged in length from 191 to 243 base pairs (bp) and correspond to scaffold_3277:pos_6-248, scaffold_9777:pos_61-260, scaffold_13129:pos_33-266, scaffold_8542:pos_18-213, and scaffold_6636:pos_71-261 of the American alligator genome (AllMis1; GCA_000281125.1; (15)).

We sampled the composite Lake Hill core at the LacCore facility (University of Minnesota) in May 2013 and October 2014. Samples for DNA analysis were collected under semi-sterile conditions: the sampling team wore gloves and facemasks and all re-usable equipment was soaked in bleach and rinsed with double distilled water. We also lined work surfaces with aluminum foil to avoid direct contact of materials with the LacCore workstations. In May 2013, we took 209 samples, by sampling every 4 cm throughout the top 836 cm of the core, and a further nine samples between 916 and 1302 cm. For each area of the core to be sampled (depth of 2 cm), we used a sterilized microscope slide to remove the top 2 mm of the exposed core drive surface. We then used a sterile, disposable 10-cm^3 syringe, with the tip removed, to core out 2 cm^3 of sediment

(as measured by the gradations on the side of the syringe). We took care not to touch the side of the core with the syringe. Rotating the syringe slightly whilst extending the plunger ensured that the sample was taken cleanly, and the plunger was used to empty the sample into a sterile, pre-labeled 50 mL falcon tube. We then sealed tubes with parafilm to reduce potential contamination and sample leakage. In October 2014, we took a further ten samples (PH167 - PH176 in Table S5) from core drives surrounding the mammoth extinction window that overlapped previously sampled depths (Fig. S5c), using the aforementioned procedure.

DNA extraction. Strict clean room protocols were adhered to at the UCSC Paleogenomics laboratory (following (16)). For each DNA extraction, we subsampled 250 mg of wet sediment from the 2 cm^3 samples. Four methods of DNA extraction were implemented, using: (1) the MoBio (California, USA) PowerSoil or (2) Powerlyzer kits, both following the manufacturer's instructions. (3) A modified version of the PowerLyzer kit protocol, in which we substituted the bead solution with Bulat buffer (17, 18), which consisted of 50 mM Tris-HCl (pH 8), 150 mM NaCl, 20 mM EDTA, 500 mM / 3.5% beta-mercaptoethanol, 50 mM DL-dithiothreitol, 2 mM N-phenacylthiazolium bromide, and 0.8 mg/mL Proteinase K. We lysed the sample overnight at 65°C with gentle agitation. The remaining protocol followed the PowerLyzer kit instructions. (4) The Andersen phenol-chloroform protocol described in (19). For all four methods, DNA was eluted in 60 to 100 μL of Tris-EDTA, with 0.05% Tween-20.

Initial PCR testing. Initial testing of DNA extracts using the PCR failed to amplify a product of the correct size. PCR was attempted on samples extracted using methods 1 and 4 using four mitochondrial DNA primer sets (two d-loop, two 16S rRNA): mam_15686F / mam_15780R (20), mam15641F / mam15721R (21), 16Smam1 / 16Smam2 (22), and 16Smam3 / 16Smam4 (23). Reactions consisted of 1× HiFi buffer, 2.4 mM $MgSO_4$, 0.8 mg/mL rabbit serum albumin, 250 μM dNTPs, 0.4 μM of each primer, and 1 U Platinum HiFi Taq (Invitrogen) for a final volume of 25 μL. The 16Smam_blkhum3 human blocking primer was included at 2 μM in reactions attempting to amplify a 16S locus (24). Cycling conditions consisted of 94°C for 12 minutes, 94°C for 30 seconds, 52°C for 45 seconds, 68°C for 45 seconds, and 68°C for 1 minute, with the middle three steps repeated for 50 cycles. Failure to amplify with PCR could indicate that the DNA extract is inhibited, or that suitable template is absent or too fragmented. Spike-in PCR experiments revealed

that inhibition was present in samples extracted with method 4, but not those extracted using method 1. We therefore moved to a high throughput sequencing approach for the detection of mammoth DNA.

DNA library preparation and sequencing. We converted DNA extracts into Illumina compatible libraries, following the Meyer and Kircher (25) protocol as modified by (26). DNA libraries were quantified using qPCR and sequenced at UC Santa Cruz on the Illumina MiSeq platform for 2×75 cycles following the manufacturer's instructions.

Initial read filtering. A total of 98 million reads were generated across the entire data set (Table S5). We trimmed adapters, merged paired end reads, and removed reads shorter than 30 base pairs, which may not map correctly, using SeqPrep (https://github.com/jstjohn/SeqPrep; flags: -o 10, -L 30, -q 15). We then removed low-complexity reads, which can align to genomes spuriously, using the DUST (27) algorithm (cutoff: 7) in PRINSEQ-lite v0.20.4 (28).

Read mapping and further filtering. To identify mammoth DNA from environmental shotgun data, we developed a pipeline to remove reads that could have originated from exogenous sources. We separately aligned merged and low-complexity filtered reads from each data set to the African elephant and Wrangel Island woolly mammoth (29) genomes (Table S6), using the Burrows Wheeler Aligner (BWA; v0.7.7) (30). We disabled the seed (-l 1024; (31)) and retained reads with a mapping quality of 20 or greater. Duplicated reads were removed with rmdup in SAMtools (v0.1.19) (32). To remove reads that may have derived from common lab contaminants (human, house mouse) or samples commonly handled in the UCSC Paleogenomics lab (horse, cow), we removed reads that mapped to the African elephant and the woolly mammoth if they also mapped to at least one of these four boreoeutherian genomes (Table S6), using the same BWA parameters described above. To further remove potential spuriously aligned reads, we compared all remaining aligned reads to the NCBI nucleotide database (release date, 2015/01/17). For this, we used BLASTn, and allowed hits with an e-value of 1×10^{-3} or lower. For these comparisons, we used Genbank identifiers assigned to Proboscidea that were downloaded on 2015/01/26. We removed reads that either exclusively matched non-proboscidean sequences or had a higher match (lower e-

value) to a non-proboscidean sequence in cases where there were hits to both Proboscidea and non-Proboscidea. Reads that could not be identified were retained.

As a negative control, we repeated this pipeline using a Hoffman's two-toed sloth genome. We modified the pipeline by using Genbank identifiers assigned to Pilosa for the NCBI nucleotide database comparisons. The two-toed sloth belongs to the Xenarthra, which is both distinct from Afrotheria and Boreoeutheria (Table S6; (33)), and a group that should not be present in the Lake Hill core. Although giant ground sloths (*Megalonyx jeffersonii*) existed in eastern Beringia (Alaska, Yukon), their fossils have only been recovered from deposits considered to be of last interglacial age (~125,000 years ago) (34) and have not been recovered from St. Paul Island (35).

Characterization of post-filtered reads. For each sampled depth, we calculated the mean and standard deviation of the proportion of merged and complexity filtered reads that were considered to be mammoth (aligned to African elephant or woolly mammoth) or 'sloth' (aligned to Hoffman's two-toed sloth), by combining available replicates (Table S5). There were four types of replicate; (1) independent DNA extraction of the same sample, (2) independent extraction of a different sample from the same composite depth, (3) independent DNA library preparation of the same extract, and (4) library sequenced twice. As we had removed duplicates from reads considered to be mammoth or 'sloth', we also removed potential PCR duplicates from unaligned (merged and complexity filtered) reads using PRINSEQ with the -derep 124 flag, which best approximates SAMtools' rmdup, for proportion calculation.

To provide support for the ancient origin of the reads considered to be woolly mammoth, we characterized the DNA damage patterns of these reads, including DNA fragment length distributions, fragmentation patterns, and deamination-induced misincorporations at the 5' and 3' ends of reads. For this, we combined reads considered to be mammoth from all data sets and conducted damage analyses of these reads, as mapped to the African elephant genome, in mapDamage v2.0.5 (36). This procedure was repeated for all reads aligned to the woolly mammoth and two-toed sloth genomes.

Alligator amplicon contamination assessment. To ensure that samples had not been contaminated by American alligator amplicons sprayed onto drilling equipment during core sampling, we aligned merged and complexity filtered reads against five references, consisting of the amplicon

sequences, using BWA under the parameters listed above. None of the reads from any of the data sets aligned to these references.

Data availability. Raw sequencing reads are available on the NCBI Short Read Archive (SRA) under BioProject accession PRJNA320875, with SRA accessions SRR3480229-SRR3480293 (Table S5). We caution that some of these data sets are likely to include sequences from boreoeutherian taxa, including bison and/or horse, as libraries from these taxa were sequenced on the same sequencing runs as those analyzed here. No other proboscidean or xenarthran-derived libraries were sequenced on these runs.

Results and discussion

Support for authenticity of mammoth DNA from the Lake Hill core. We argue that the majority of the sedaDNA data we have assigned to mammoth is authentic, based on two grounds: damage analysis of mammoth reads and a far fewer, but relatively consistent, number of reads assigned to a negative control species.

Analysis of DNA damage patterns can be considered a robust method of assessing if DNA looks 'ancient' (37). Ancient DNA is often characterized by a short mean fragment length (often less than 100 bp), an excess of cytosine to thymine deamination-induced misincorporations at the 5' end of reads, and an excess of purines (adenine, guanine) in the base immediately upstream of the 5' end of the read (38). For the latter two signatures, a corresponding increase in guanine to adenine misincorporations at the 3' end of reads and an excess of pyramidines (cytosine, thymine) in the base immediately downstream of the 3' end of the read may be observed, due to damage on the opposite strand. All of these characteristic ancient DNA damage signatures are observed in the Lake Hill sedaDNA data set for reads assigned to mammoth based on alignment to both the African elephant and woolly mammoth genomes (Fig. S6).

As a negative control to quantify the rate of random read mapping, we repeated our pipeline based on alignment to Hoffman's two-toed sloth. This species falls outside of the diversity of Boreoeutheria, which includes common contaminant taxa and species regularly processed in the clean lab at UC Santa Cruz, and is highly diverged from Proboscidea (Table S6; (33)). Although nearly all samples contained reads that aligned to the two-toed sloth and passed all filters, these

numbers are far lower than those passing for woolly mammoth in samples from below, or older than, the mammoth extinction window (502-503 cm, MCD; Fig. S5a, Table S5). In samples from above the mammoth extinction window, however, the proportion of reads assigned to the two-toed sloth and woolly mammoth are broadly similar. Further, these proportions from above the mammoth extinction window are similar to those observed from two negative DNA extraction controls. Reads assigned to the two-toed sloth do not display the damage patterns expected from authentic ancient DNA (Fig. S6g-i).

Although it is reasonable to consider 'mammoth' reads to be of mammoth origin, based on sample age and provenance, it seems counterintuitive that more reads would align to the African elephant rather than the woolly mammoth genome (14142 and 11785 reads, respectively; Fig. S5b). We suggest that this is an artifact of genome completeness, which is supported by the proportion of uncalled sites (Ns) in these genomes: the African elephant has a lower proportion of uncalled sites (2.45%) compared to the woolly mammoth (9.84%).

Timing the loss of mammoth sedaDNA from the Lake Hill record. Prior to the mammoth extinction window, mammoth DNA is found in far higher proportions than in both the extraction and alignment negative controls (Figs. 2, S5a, Table S5), which suggests that mammoths existed in the vicinity of the Lake Hill lake during this sampled interval, ~10,900 (718 - 720 cm, MCD) to 5,600 (502 cm, MCD) cal. years BP. Immediately after the mammoth extinction window, however, the proportion of DNA assigned to mammoth becomes broadly similar to the negative controls. We therefore infer that mammoth were absent from the Lake Hill region after 5,600 cal. years BP. The transition between the presence and absence of mammoth DNA coincides with the loss of coprophilous fungal spores (*Sporormiella*, *Podospora*, *Sordaria*; Fig. 2), which are an independent proxy for mammoth presence, from the Lake Hill core record.

S6. Coprophilous spores and pollen

Materials and methods

The abundance of coprophilous spores was employed as a proxy for mammoths and pollen abundance in the composite core yielded relative accumulation rates of herbs and shrubs. Initial sampling resolution for spore and pollen samples was at 16 cm intervals throughout the core but

with higher resolution sampling for selected intervals: 4 cm resolution at 0-33 cm (MCD) to detect the timing of reindeer introduction on St. Paul Island, 8 cm resolution at 400-480 cm and 520-650 cm to better understand vegetation change before and after the woolly mammoth extinction, and at 4 cm and 2 cm resolution at 480-493 cm and 493-520 cm, respectively, to detect the timing of woolly mammoth extinction. In total, 81 1-cm^3 sediment samples were taken for pollen and spore analysis, as measured by a volumetric metal syringe.

Extraction and processing of spores and pollen followed a modified version of the University of Minnesota Limnological Research Center protocol (39). These modifications included the addition of 1 mL of polystyrene microspherule solution (5.0×10^4 sph/mL ± 8%) to calculate pollen concentrations and accumulation rates. Samples were sequentially incubated in (1) 10% HCl in boiling water for five minutes to remove carbonates, (2) 10% potassium hydroxide for 10 minutes to break up sediment and to remove humic acids, (3) 48% hydrofluoric acid for 20 minutes in boiling water to remove silicates, and (4) Erdtmann's acetolysis solution (concentrated sulfuric acid and acetic anhydride at a 1:9 ratio) for two minutes in boiling water to remove organic materials (cellulose), clean the surface of the spore and pollen grains, and etch the grains to ease identification. All samples were transferred to dram shell vials filled with silicone and slides were prepared by placing one drop of sample onto the slide and adding a cover slip, which was then sealed with fingernail polish. Each pollen sample was scanned at 400 × magnification (or 1000 × magnification with oil immersion, if necessary) and counted and identified at least 300 pollen grains. Pollen and spore abundances were expressed as accumulation rates (grains yr^{-1} cm^{-2}).

Results

We conducted pollen analysis to infer late-glacial vegetation changes on St. Paul Island and coprophilous spore analyses to infer the timing of mammoth population declines and extinction. Prior palynological research (40) indicates that the main pollen taxa on St Paul Island during the Holocene are *Artemisia*-type, Poaceae, Cyperaceae, Apiaceae, *Salix*-type and *Empetrum*. The changes in abundances of shrub and herb/grass pollen types indicate vegetation shifts between shrub-tundra and herb/grass-tundra on the island. The pollen taxa identified from the Lake Hill composite core are listed in Table S7. Three types of coprophilous fungi spores – *Sporormiella*-

type, *Podospora*-type, and *Sordaria*-type – were used to detect woolly mammoth population declines. In addition to the occurrences of these spores outlined in the main text, isolated single spores of *Sporormiella* and *Sordaria* occurred at 4,880 ± 85 and 920 ± 120 cal. years BP, but are regarded as unreliable indicators of mammoth presence. They could have resulted from the reworking of older sediments, from spores on fox or shrew dung, or by long-distance wind transport from mainland sources.

S7. Macrobotanical remains

Materials and methods

Plant macrofossils were sampled to infer late-glacial floristic patterns on St. Paul Island, augmenting the results from the pollen analyses described above, and to provide organic material for AMS ^{14}C dating. The composite core was sampled every 10 cm, but shifted to finer resolution (sampling every 2-5 cm) for the lower portions of the core (Table S2). We removed 2 cm^3 samples from the composite core, which were placed directly in small Nalgene vials with snap-tight lids. Additionally, if any visible macrobotanical specimens were identified during core sectioning and sampling for other proxies, these were recorded, isolated, and placed in sterile glass vials filled with distilled water for AMS ^{14}C dating (as described previously).

Each sediment sample was placed into a glass petri dish and enough distilled water was added to gently disaggregate and separate sample constituents. Sieving was avoided due to small sample volumes and potential contamination for AMS ^{14}C dating. Each sample was scanned under incident light at 10-60 × magnification. Individual plant macrofossil specimens were manually extracted with metal forceps or a spatula and transferred to sealed glass vials filled with distilled water. Leaf cuticles in glycerin solution were mounted on glass slides under cover slips for direct observation of the stomata and other anatomical details. Wood specimens were analyzed by preparing transverse and longitudinal (radial and tangential) thin sections using steel microtome blades, and individual sections were mounted in glycerin solution on glass slides. Wood sections and leaf anatomy were analyzed by transmitted-light microscopy at magnifications ranging from 100-1000 ×.

Vascular plant propagules and leaf tissues were identified with reference to comparative specimens collected on St. Paul Island in summer 2013, a small herbarium voucher collection at

the St. Paul school library, the online LacCore photographic plant macrofossil reference collection, and relevant published sources (41-46). Wood identification was based on the three-dimensional anatomical characteristics, employing published keys (47), the online anatomical database (48, 49), and comparison to material collected during the fieldwork on St. Paul. We assigned Arctic willow (*Salix* sp.) wood based on the presence of simple perforation plates, medium sized, alternate inter-vessel pitting, and heterocellular rays with very coarse ray-vessel pitting. *Salix* leaves were assigned from the leaf architecture (cross-venulate venation pattern), sclarification of vascular bundle fibers, and anomocytic stomata. Lower vascular plant and bryophyte identifications were based on published sources (50, 51), online resources (52-54), and the LacCore photographic collection.

In general, plant macrofossil remains were few and sparsely distributed throughout the composite core. Individual item counts per sample, rather than quadrat counts or abundance estimates (55, 56), were therefore used.

Results

A total of 140 samples were analyzed, resulting in 14 taxonomic assignments. Among these are mosses (Bryopsida, four to five taxa), two graminoids (*Carex*, *Juncus*), one mustard (*Draba*), five provisionally identified forbs, and two shrubs (*Salix* and *Empetrum*) (Table S8).

Willow (*Salix* sp.) and moss remains were fairly regularly present among the core samples, however the former was not observed below 780 cm. Moss gametophore fragments comprised the most abundant and common plant remains overall. The majority of this material was highly fragmented. When considered according to Janssens's (57) classification scheme (hierarchic preservation classes for fossil bryophyte fragments on a scale of 0-10), most specimens conform to classes 1 through 6 (leafless stems, branching infrequently preserved, leaves primarily loose and in fragmentary condition).

S8. Diatoms and Cladocerans

Materials and methods

Preparation of diatom samples followed a modified protocol (58) with each sample between 0.1 and 0.2 g of non-calcareous wet sediment treated with 5 mL of 30% hydrogen peroxide, which was left to digest for one week before being rinsed several times with distilled water. Dilutions of the resulting slurries were pipetted onto cover slips and left to dry at room temperature before being permanently mounted onto glass slides using Meltmount™, a thermal plastic with a refractive index similar to Naphrax (1.704). A minimum of 400 diatom valves were enumerated from each sample using a Leica DM microscope (Laboratoire de paléoécologie aquatique, Université Laval) at 1000 × magnification under oil immersion. Keys consisting mainly of northern North American floras (59-61) assisted in identification to the lowest possible taxonomic level.

Cladocera were processed using an adapted version of a previously described method (62). Sediment samples were deflocculated in a 10% solution of potassium hydroxide and the 125 and 65 μm fractions were isolated by sieving. The retained chitinous remains were transferred into vials using distilled water and stained with Safranin solution. Aliquots of 1 mL were pipetted onto a Sedgewick-Rafter cell and a minimum of 150 individuals for each sample were counted using a compound microscope at 400 × magnification. Cladocerans were identified using keys (63-66) to species, wherever possible. The most numerous sclerites (i.e. carapace, post-abdomen or head-shield) were employed to calculate the number of individuals of each species and expressed as percentage relative abundance. This separation of the exoskeletal remains can make it difficult to identify certain taxa to species level. For the purposes of this study, *Bosmina longirostris* (Müller 1785) and *Eubosmina longispina* (Leydig 1860) were grouped *Bosmina* spp., as the species can only be distinguished from the positioning of the lateral head pore, which is not always visible. Unidentifiable small and medium-sized *Alona*-type head shields and carapaces were grouped as *Alona* spp. (not included in Fig. S7), as were *Chydorus* spp., and *Daphnia pulex* agg.

We conducted Bayesian change point (BCP) analyses on the cladoceran and diatom data to identify likely locations of abrupt change points in the time series. Analyses were conducted in R, using a combination of *Bacon 2.2* (67) and *bcp* (68) for the change-point analyses.

Results

Diatoms. Prior to 7,850 cal. years BP, MCD, high lake levels and oligotrophic conditions are indicated by a diatom assemblage dominated by the small planktonic freshwater taxon *Discostella pseudostelligera*, along with benthic freshwater taxa *Stauroforma exiguiformis* and *Psammothidium curtissimum*. In mainland Alaskan lakes, *D. pseudostelligera* has an optimal water depth of 9.4 m and a low total phosphorous (TP) optimum (8.8 μg L^{-1}) (69). *D. pseudostelligera* abundances decrease rapidly from around 7,550 cal. years BP and it disappears between 7,170 and 6,770 cal. years BP. The following period was dominated by an assemblage of benthic and tychoplanktonic diatom taxa with optimal depths around 5.6 – 4.2 m and slightly higher (~ 12-14 μg L^{-1}) TP optima (69). This assemblage includes high relative abundances of *P. curtissimum*, which favours sandy substrates and is the most common taxon between 7,850 and 5,600 cal. years BP, *S. exiguiformis*, and *Staurosira construens* var. *venter*, which are tolerant of high conductivity (69) and salinity (70, 71), shorter growing seasons, and higher turbidity in the water column. Fig. S8. presents the sedimentary diatom data and includes all taxa (or groups) with relative abundances of at least 10% in any particular sample. BCP analysis indicates likely change points at a) 6,490 cal. years BP, marking the decline in planktonic diatoms and increase in conductivity-tolerant diatoms, b) 6,050 cal. years BP, marking the increase in tychoplanktonic diatoms, and c) 5,490 cal. years BP, marking a decline in conductivity-tolerant and tychoplanktonic diatoms.

Cladocerans. Cladocerans from the Lake Hill composite core are also consistent with a reduction in lake depth and deterioration in water quality to more turbid with higher ion concentrations. Prior to 6,670 cal. years BP, the lake was dominated by the pelagic species *Bosmina longirostris* and *Eubosmina longispina*. The dramatic switch in dominance to littoral and benthic cladocera and the negligible occurrence of any pelagic taxa after 6,265 cal. years BP suggests a significantly and permanently lowered lake level. During this sharp transition *Alona circumfibriata* Megard 1967, which has demonstrated resilience to fluctuating salinity (72-74), dominated the species assemblage (68%), being extirpated by *Chydorus* and *Alona guttata* Sars 1862 by 5,326 cal. years BP. Although these benthic taxa are also tolerant of high electrolytic conductivity, *Alona barbulata* Megard 1967 and *Alona quadrangularis* O. F. Müller 1775 declined (<1%). These taxa are typically found in athalassic lakes (75) and only reappeared after 3.359 cal. years BP. The full biostratigraphy for the cladoceran data is shown in Fig. S8, which is color coded to match the

figure in the main body of the text. BCP analyses indicate likely change points a) in the ratio of pelagic to littoral cladocerans at 6,430 cal. years BP, marking declining proportions of pelagic cladocerans, b) *Alona circumfibriata* at 6,420 cal. years BP, marking its increase, and c) *Alona circumfibriata* at 5,390 cal. years BP, marking its decline.

S9. Isotopic analyses

Materials and methods

The oxygen isotope compositions (expressed as $\delta^{18}O$ values) of chironomid head capsules and other aquatic insect chitin were processed and analyzed at the Alaska Stable Isotope Facility (ASIF), University of Alaska Fairbanks using previously published protocols (76, 77). Samples were processed from core sections at a 4 cm resolution. After freeze-drying, samples were placed in an autosampler attached to a TCEA-IRMS system for analysis. All $\delta^{18}O$ values are expressed relative to Vienna Standard Mean Ocean Water (VSMOW) and have an analytical precision of 0.1 per mil (‰) based on previously published protocols (77).

Bulk sediment samples were collected from the core at 16 cm intervals for other isotopic and geochemical analyses. Methods followed previously published protocols (78) for analyses of stable carbon and nitrogen isotopic compositions of total organic matter (expressed as $\delta^{13}C$ and $\delta^{15}N$ values respectively), elemental analysis of total organic carbon (TOC) and total nitrogen (TN), and calculation of C:N ratios using a Costech ESC 4010 elemental analyzer interfaced via a ThermoConflo III to a Thermo Delta+XP IRMS. Analytical precisions for $\delta^{15}N$, $\delta^{13}C$, TOC, and TN values were assessed using previously published protocols (78) and were 0.3‰, 0.3‰, 2%, and 1% respectively. $\delta^{13}C$ values are expressed relative to Vienna Pee Dee Belemnite (V-PDB) and $\delta^{15}N$ values are expressed relative to atmospheric nitrogen (AIR).

We analyzed the isotopic data using a combination of two-sample t-tests and linear regression. Two-sample t-tests were employed to test whether mean values before the extinction (i.e. for the population of data points from 11,200 to 5,600 cal. years BP) were significantly higher than mean values after the extinction (i.e. for the population of data points from 5,600 to -63 cal years BP). Linear regression analyses were employed to test whether apparent slopes in time series were significantly different from zero, and were fitted to the entire time series (from 11,200 to -63 cal years BP). All statistical analyses were carried out in R, using standard functions.

Results

Isotopic proxy data obtained from analyses of the Lake Hill sediments show that environmental shifts occurred around the time of the extinction of woolly mammoth on the island. These include significant changes in $\delta^{15}N$ values from analyses of total nitrogen (TN) from the sediments between 7,600 and 5,200 cal. years BP. The $\delta^{15}N$ values exhibit an abrupt enrichment (6.7‰) at 7,000 cal. years BP and then decrease, reaching a minimum value (-0.3‰) at 5,400 cal. years BP. The $\delta^{13}C$ values from analyses of total organic carbon (TOC) from the sediments and $\delta^{18}O$ values from analyses of aquatic invertebrate chitin preserved in the sediment both gradually increase from 8,000 to 5,500 cal. years BP, reaching maxima ($\delta^{13}C_{TOC}$ = -17.2‰ and $\delta^{18}O$ =16.8‰) at ~5,200 cal. years BP, indicating decreasing effective moisture during this time period. An abrupt peak in C:N values at 5,400 cal. years BP is coincident with the approximate timing of the extinction of woolly mammoth, and indicates an abrupt input of terrestrially-derived organic matter (Fig. S9.). A two-sample t-test of the $\delta^{18}O$ indicates that $\delta^{18}O$ values after the extinction are significantly higher than values during the extinction ($p= 9.378x10^{-15}$), consistent with an increasing evaporation to precipitation ratio. A t-test cannot be applied to the $\delta^{15}N$ data for the simple reason of no fossil remains exist after the extinction. We instead analyzed the $\delta^{15}N$ data using simple linear regression and found suggestive but inconclusive evidence for progressive enrichment of the nitrogen isotopes prior to extinction ($p=0.0697$ for the null hypothesis that the slope is indistinguishable from zero, so we cannot confidently reject the null hypothesis). To avoid cherry-picking data, we did not exclude the initial high value at the start of the $\delta^{15}N$ time series. Hence, our finding of no significant trend in the $\delta^{15}N$ time series is conservative, and does not rule out the possibility of a significant trend beginning after 9,000 cal. year BP.

Supplementary Figures

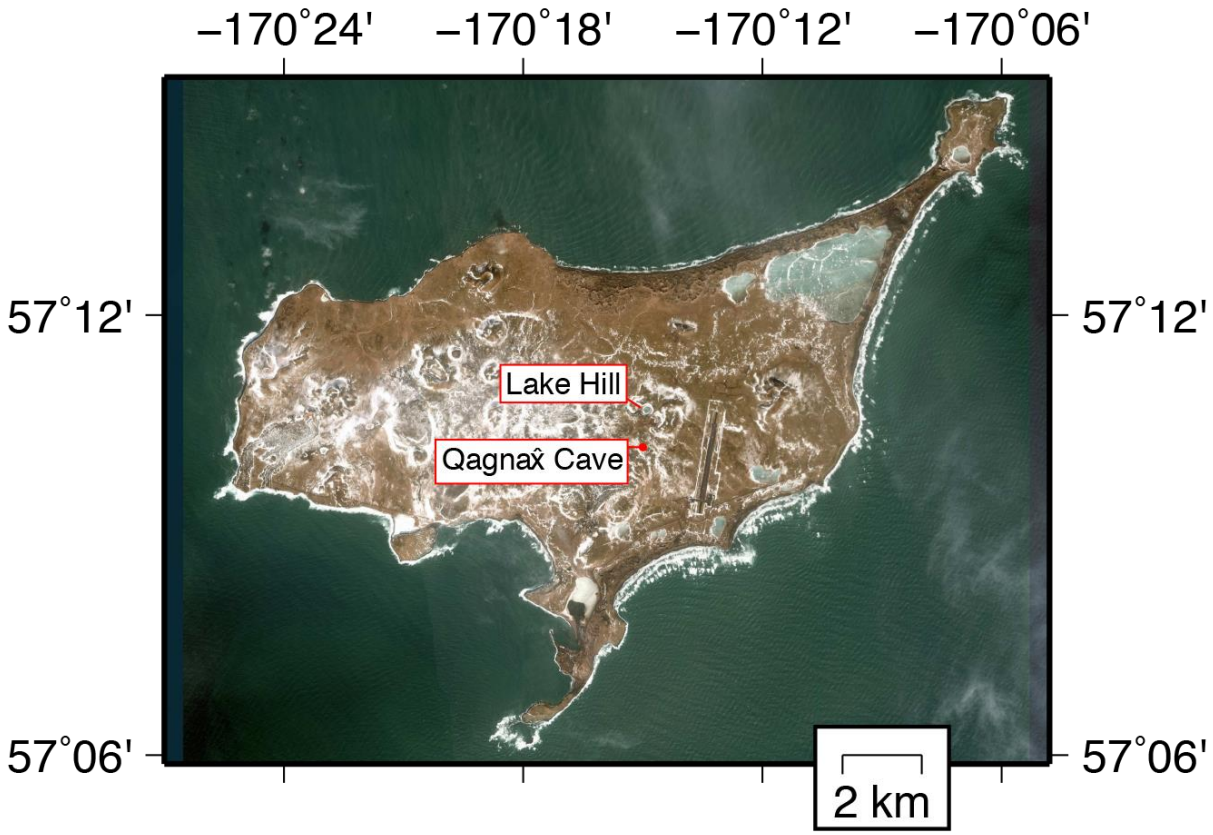

Fig. S1. Map of St. Paul Island. The sedimentary record of Lake Hill lake (highlighted) was used as the basis for the majority of the analyses of this study. Qagnax Cave (also highlighted) has previously yielded woolly mammoth fossils.

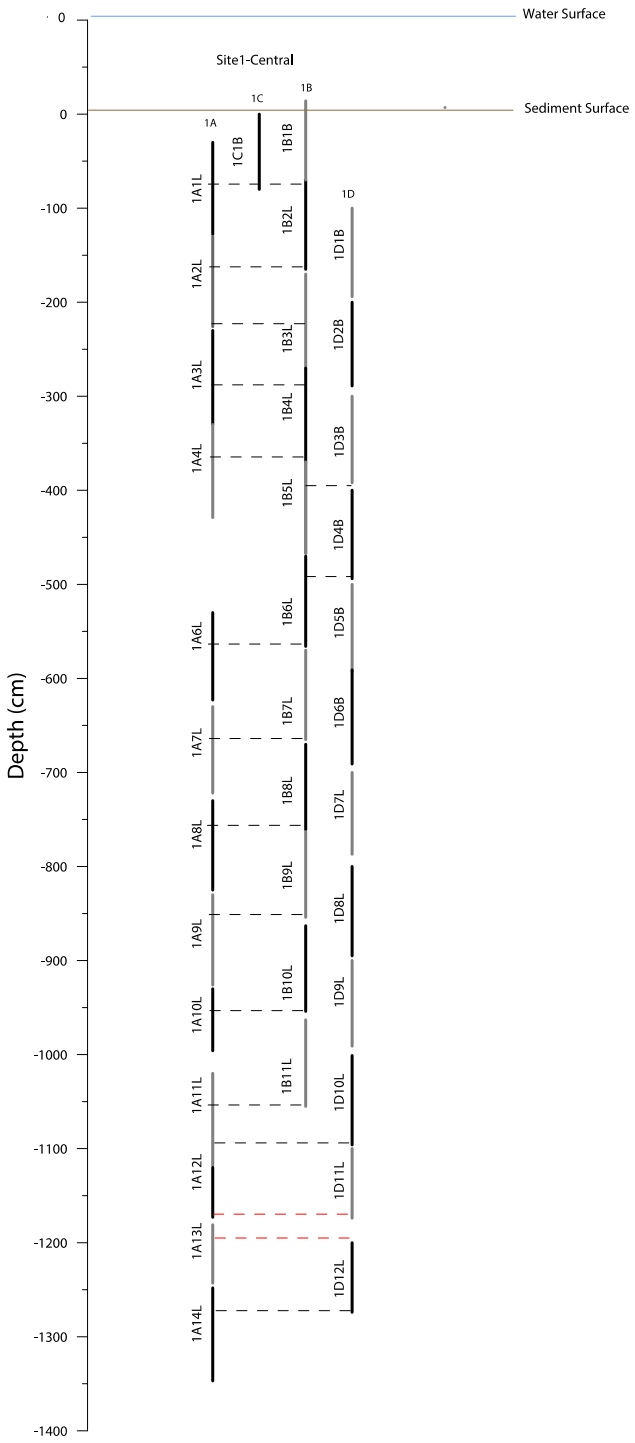

Fig. S2. Core sites sections and overlap in the composite Lake Hill sedimentary record. The composite core reached a depth of 1356 cm. One main core (section 1A) and two overlap sections (1B and 1D) were extracted to provide a continuous record. The section 1C1B corresponds the water-sediment surface core. The dashed lines indicate the shifts of overlapping sections. The red-dashed line indicates a gap in the overlap at the bottom of the coring series.

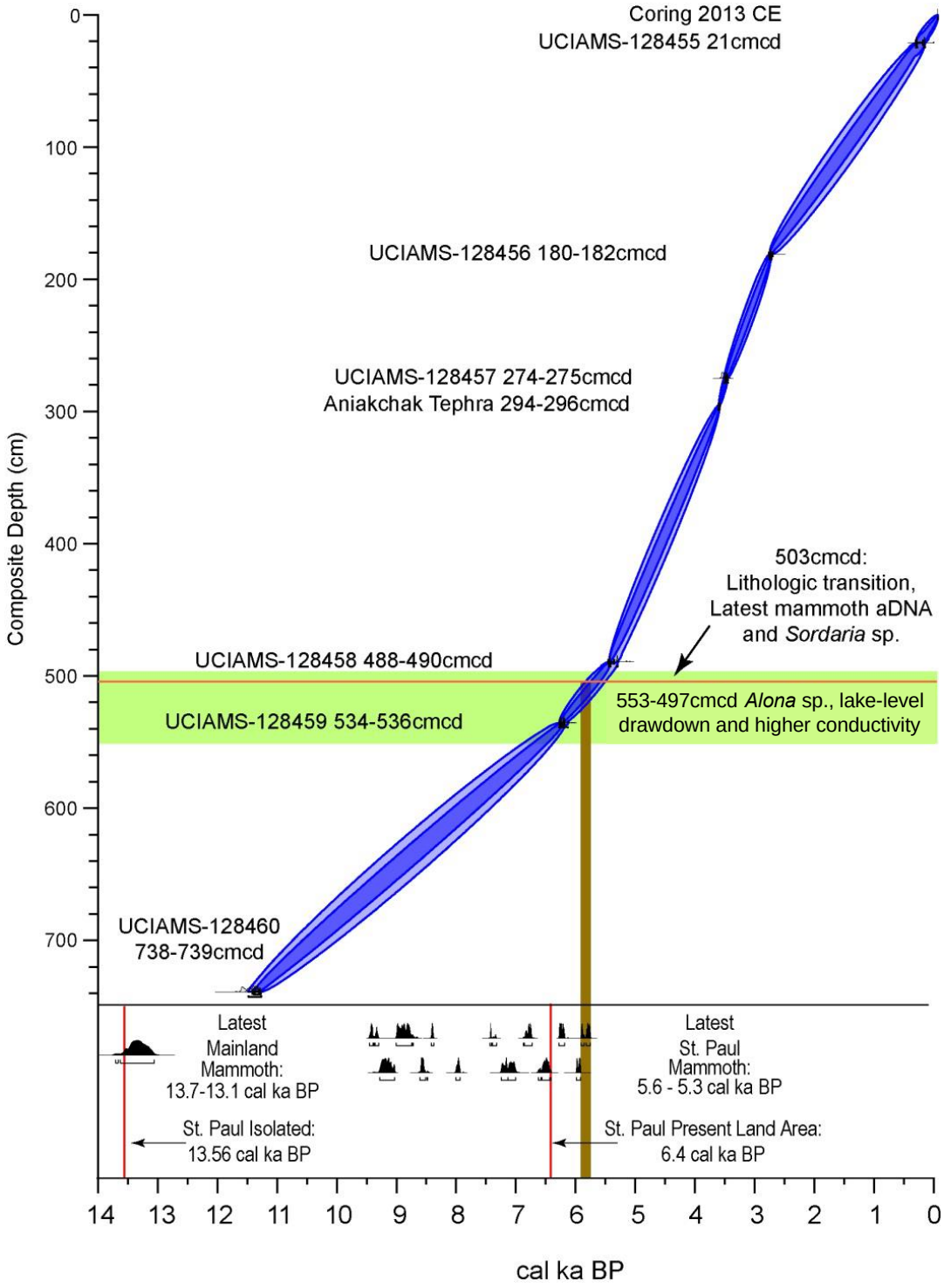

Fig. S3. The age-depth model for the upper 740 cm of the Lake Hill sedimentary record. AMS ^{14}C dates are given in Table S3. All radiocarbon dates at the bottom of the plot, including the latest mammoth dates (5,600-5,300 cal. years BP), are based on ultrafiltered bone collagen from mammoth fossils in Table S1.

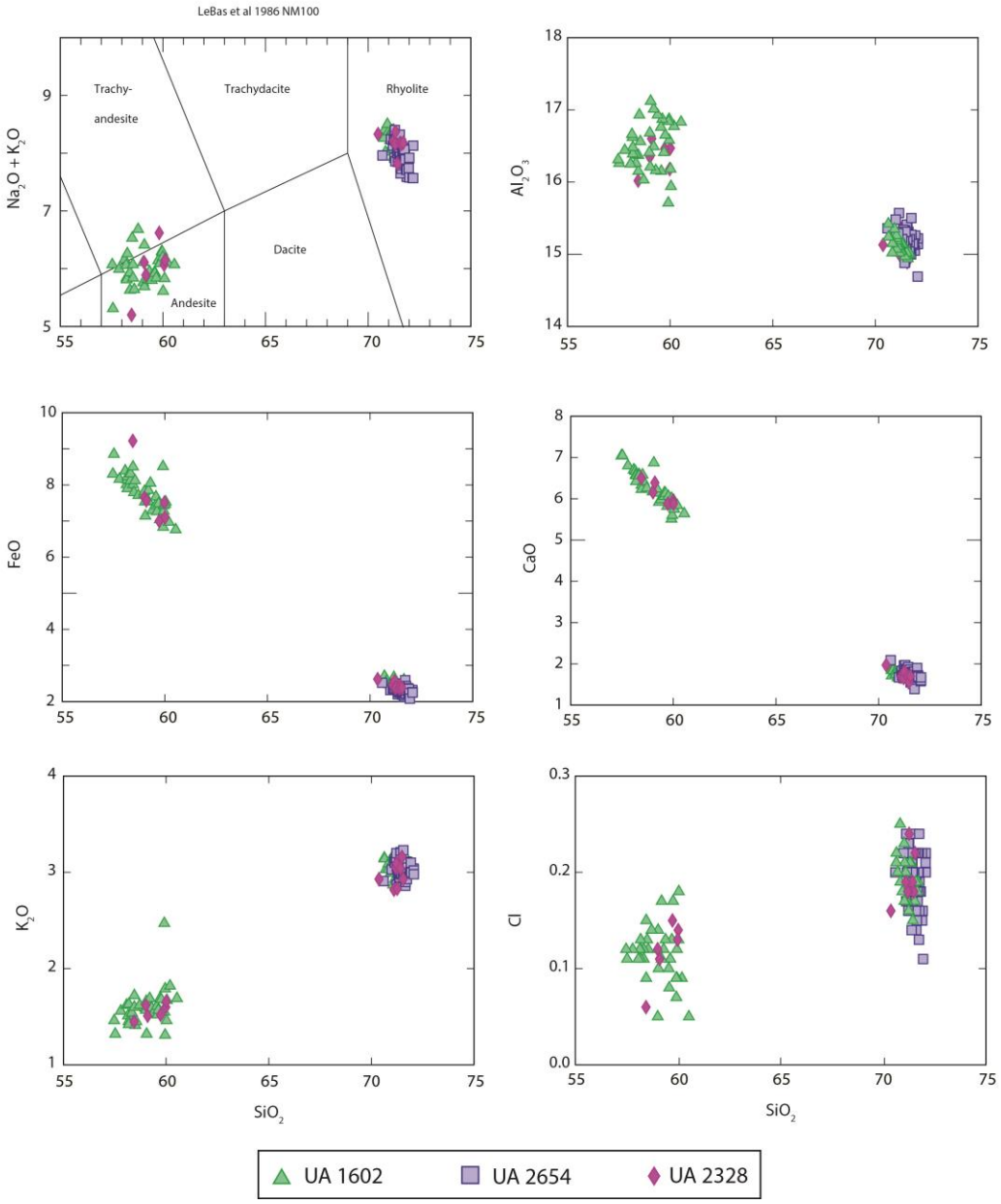

Fig. S4. Major element glass geochemical plots of St. Paul Lake Hill tephra samples (294 cm MCD; UA 2328, 2654). Aniakchak CFE II reference material (UA 1602; Zagoskin Lake, Alaska) is characteristically bimodal and both populations are present in the St Paul samples, although the higher SiO_2 rhyolite is more common.

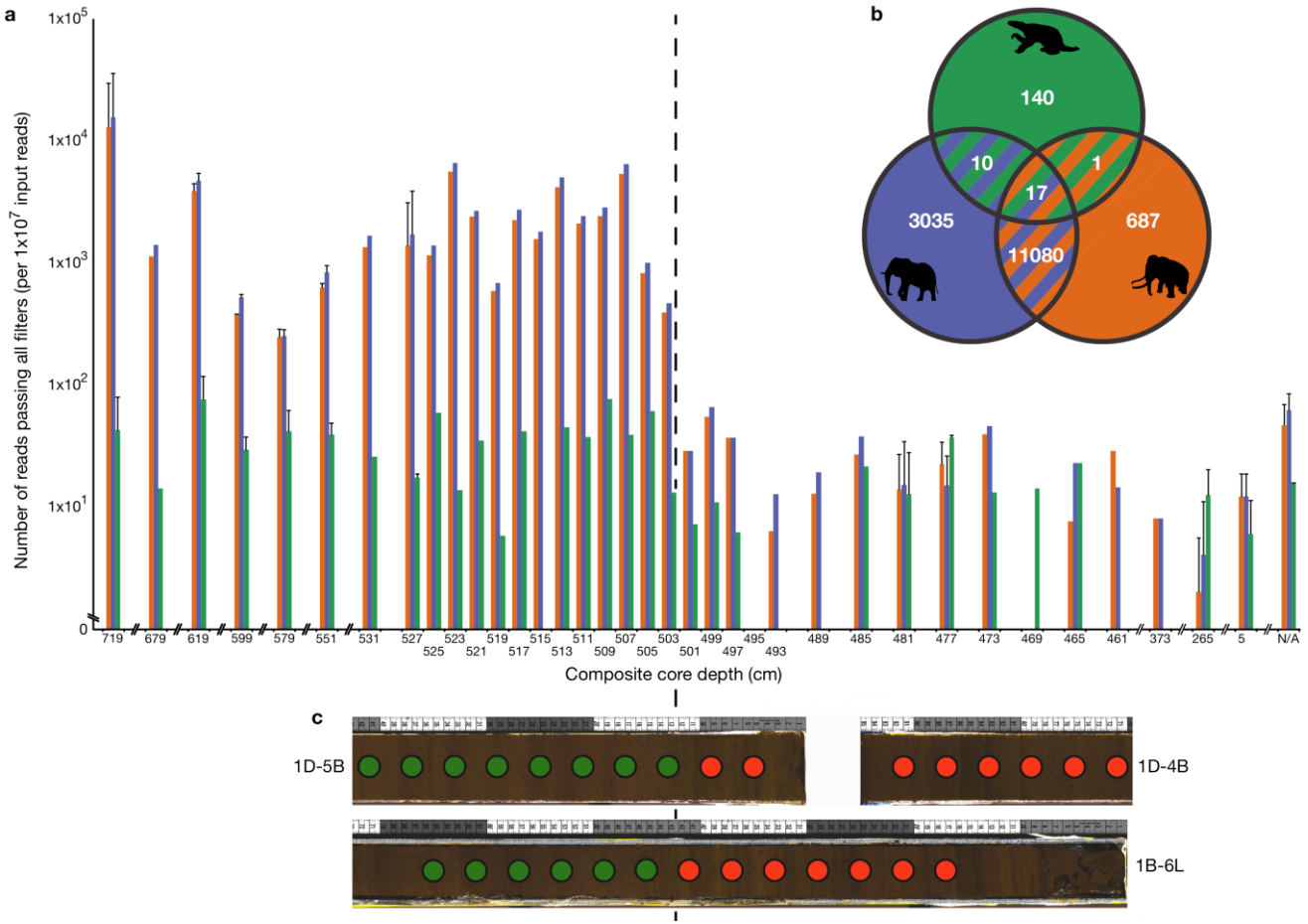

Fig. S5. The proportion of DNA molecules assigned to mammoth fall to background levels after ~502 to 503 cm (MCD; indicated by the dotted line). (a) At each sampled depth, the mean and one standard deviation of the proportion of unique DNA molecules assigned to, woolly mammoth; orange, African elephant; blue, and Hoffman's two-toed sloth; green. (b) A Venn diagram illustrating the total number of reads shared either between reference genomes (within the overlaps between circles) or uniquely assigned to each reference genome (outside of circle overlaps). The color scheme follows (a). (c) DNA sampling locations from the three cores that surround the mammoth extinction window, with green and red indicating inferred mammoth DNA presence and absence, respectively. N/A: results from two negative extraction controls. African elephant and two-toed sloth silhouettes are from http://phylopic.org and are under license at http://creativecommons.org/licenses/by/3.0/ (African elephant credit; Jan A. Venter, Herbert H. T. Prins, David A. Balfour, and Rob Slotow (vectorized by T. Michael Keesey)).

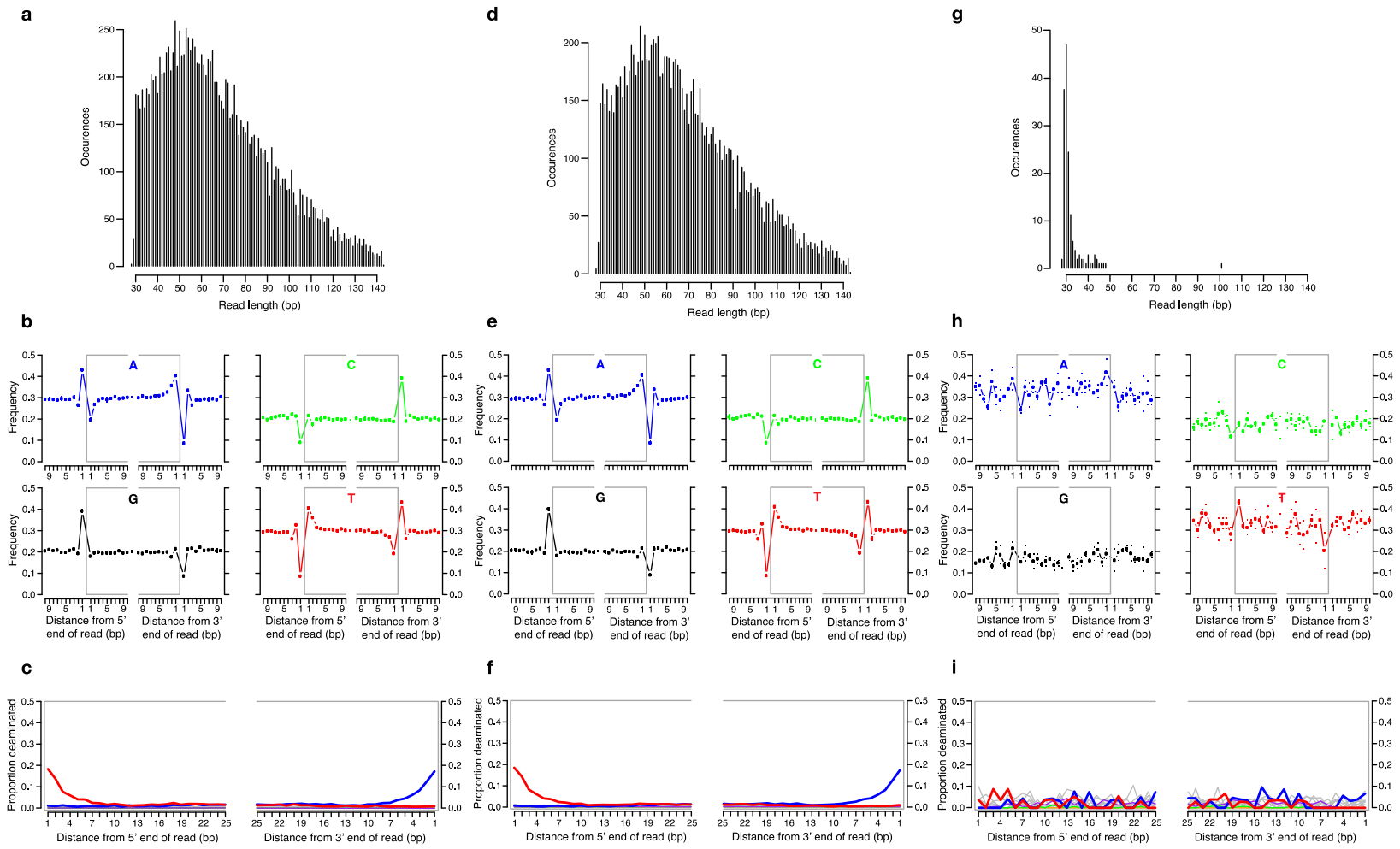

Fig. S6. DNA damage characterization of reads considered to be of mammoth (a-f) or random read mapping (g-i) origin. Fragment length distributions, fragmentation patterns, and deamination-induced misincorporation rates of reads aligned to African elephant (a-c), woolly mammoth (d-f), or Hoffman's two-toed sloth (g-i). In (c), (f) and (i), red and blue lines are rates of cytosine to thymine and guanine to adenine misincorporations, respectively.

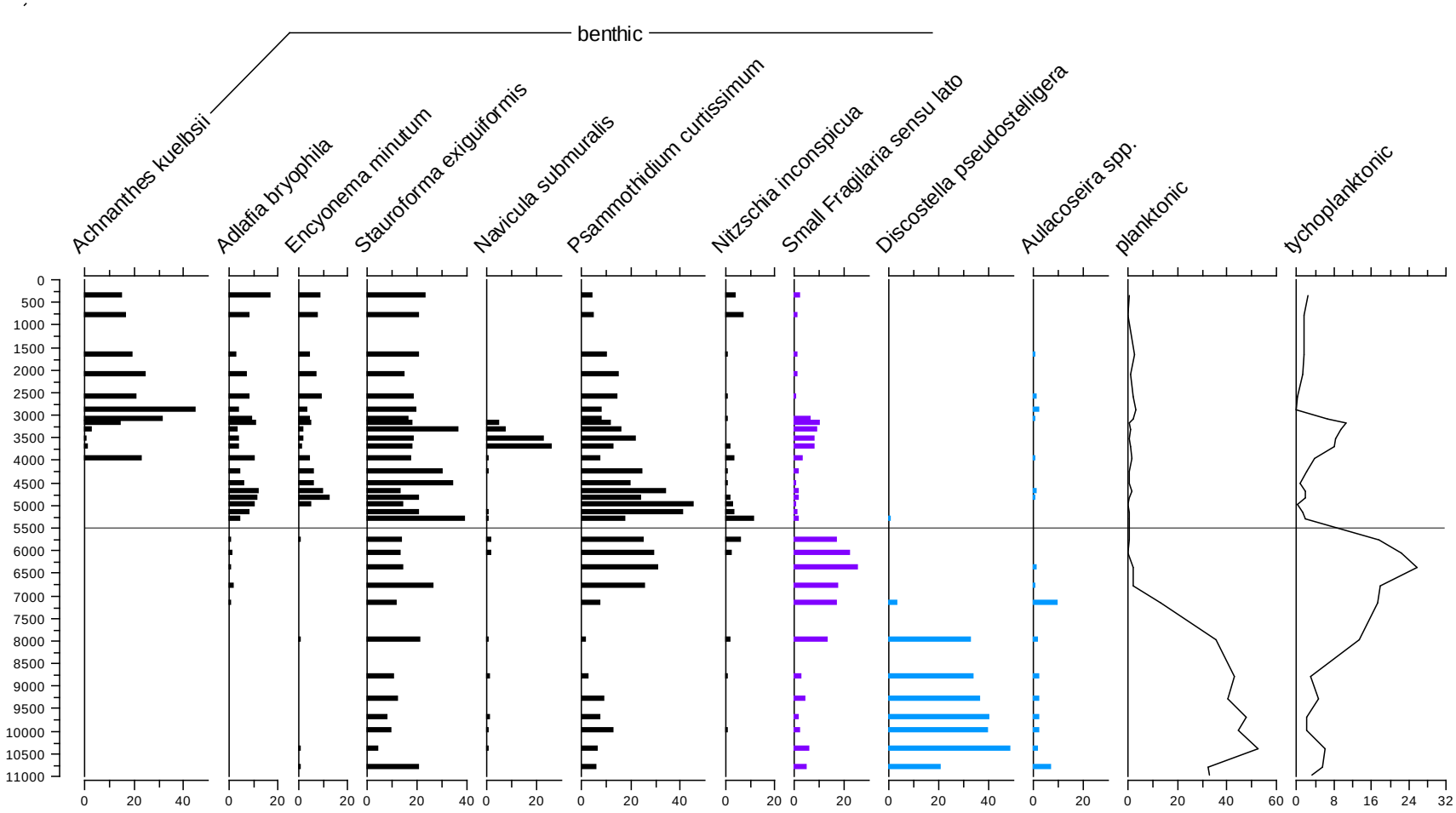

Fig. S7. Diatom biostratigraphy showing changes in relative abundances (%) for diatoms from the Lake Hill core (with all taxa over 10% relative abundance shown) against cal. years BP.

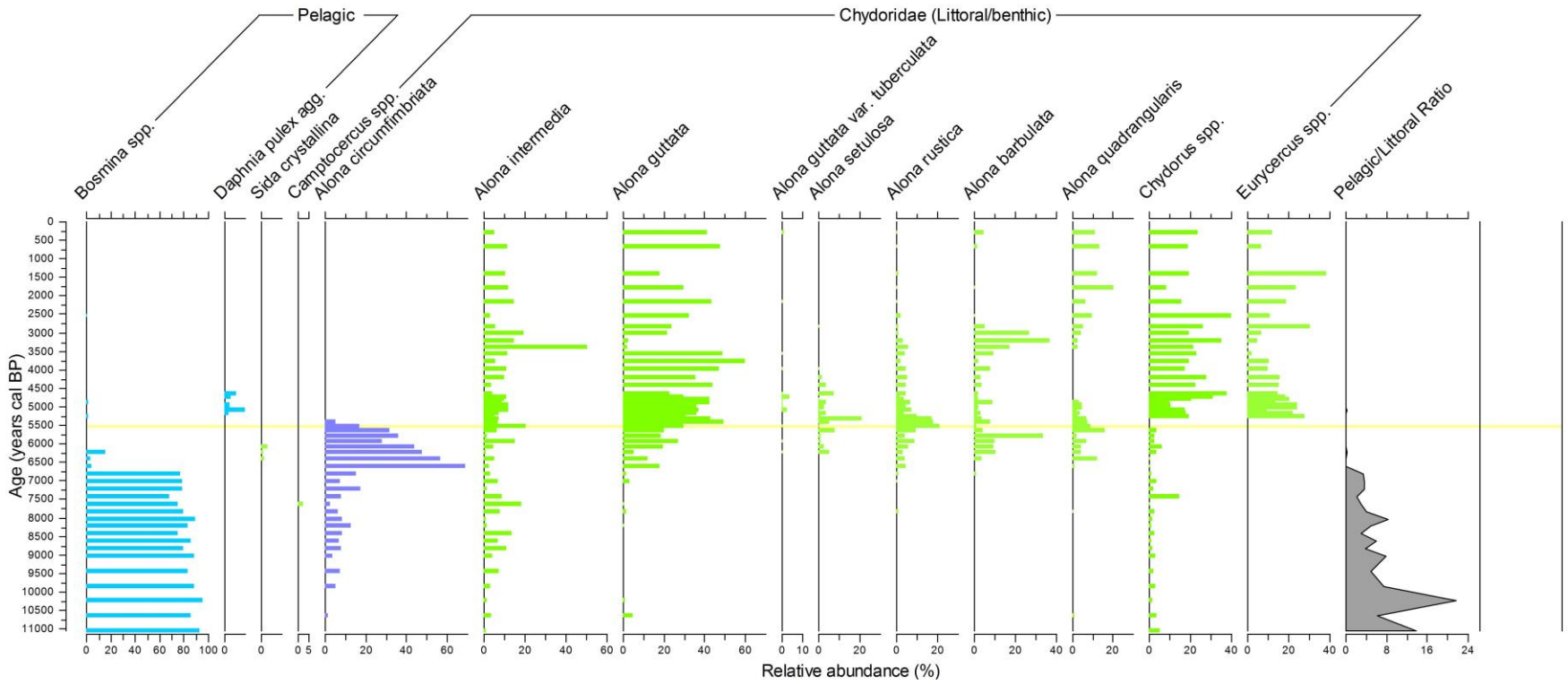

Fig. S8. Cladoceran biostratigraphy summarizing the relative abundances (%) for the Lake Hill core, with pelagic taxa in blue and littoral/benthic taxa in green. *Alona circumfibriata* is color coded as in Fig. 3.

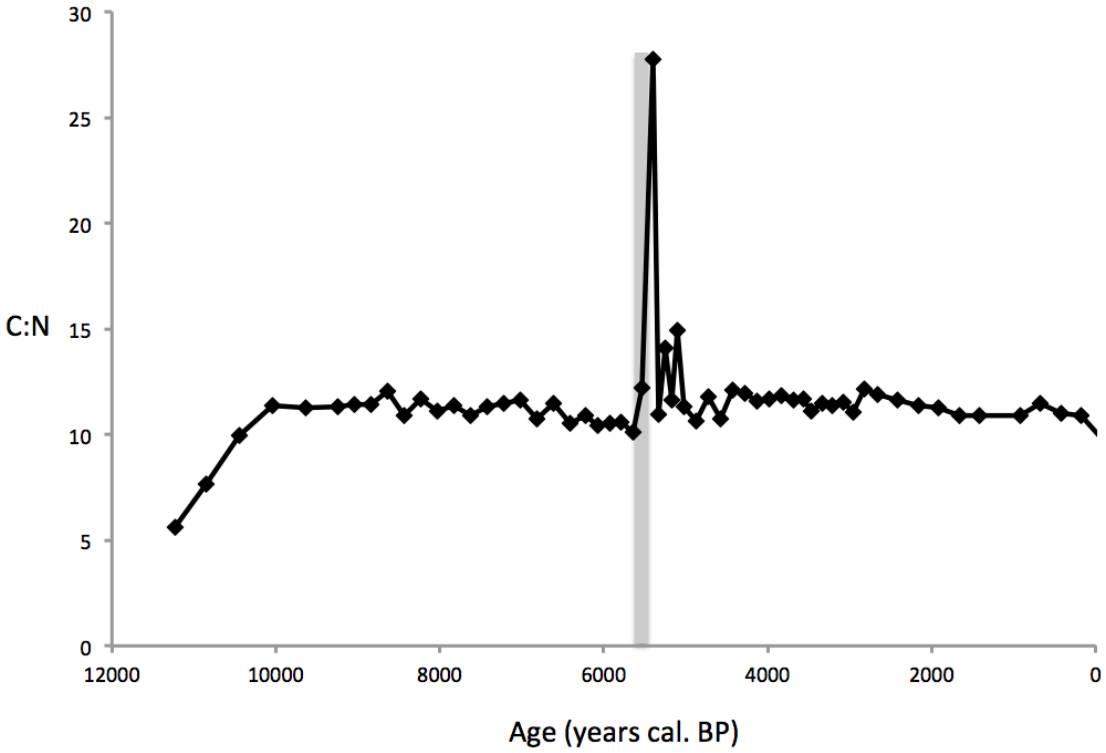

Fig. S9. C:N ratio of sediment from Lake Hill core vs. calendar years BP (grey area = mammoth extinction).

Supplementary Tables

Table S1. Radiocarbon dates derived from woolly mammoth fossils found on St. Paul Island.

Lab ID	$\delta^{13}C$ (‰)	$\delta^{15}N$ (‰)	%C	%N	C:N	Material dated	^{14}C Age (BP)	Calibrated Age Range (BP)*	Museum catalogue number	Source Study
UCIAMS-149817	-20.5	8.1	39.5	14.2	3.24	Tooth Plate	4750 ± 20	5585 - 5330		Present Study
UCIAMS-148202	-20.7	7.3	45.0	15.4	3.40	Tusk	5050 ± 20	5895 - 5735	EMS 419629	Present Study
UCIAMS-148200	-20.3	6.3	43.8	16.0	3.19	Tusk	5095 ± 20	5915 - 5750	EMS 419630	Present Study
UCIAMS-149816	-20.3	7.6	39.7	14.2	3.25	Tooth Plate	5200 ± 20	5990 - 5915		Present Study
UCIAMS-149818	-19.7	7.1	45.5	16.7	3.18	Tooth Plate	5405 ± 20	6280 - 6185		Present Study
UCIAMS-119831	-19.5	8.3	42.3	15.5	3.19	Tusk	5715 ± 30	6630 - 6410	EMS 419631	Present Study
QC: Beta-190141A						Tooth Plate	5710 ± 60	6660 - 6350		(35)
QC: Beta-190141B						Tooth Plate	5630 ± 40	6490 - 6310		(35)
QC: Beta-190141C						Tooth Plate	5770 ± 40	6670 - 6470		(35)
QC: CAMS-101895						Tooth Plate	5740 ± 35	6640 - 6445		(35)
QC: Beta-190142	-20.2	5.3				Postcranial	5800 ± 80	6785 - 6410		(35)
QC: Mean (n=5)							5720 ± 30	6635 - 6435		
UCIAMS-149815	-19.2	7.2	43.2	15.6	3.22	Tooth Plate	5960 ± 20	6880 - 6730		Present Study
Beta-213000	-18.7					Tusk	6220 ± 40	7255 - 7005		(79)
UCIAMS-148201	-19.2	7.8	46.1	16.2	3.32	Tooth Plate	6490 ± 20	7440 - 7325	EMS 419632	Present Study
UCIAMS-148199	-20.2	6.8	40.5	14.7	3.22	1st Molar	7145 ± 25	8015 - 7935	EMS 419633	Present Study
UCIAMS-149811	-19.1	4.4	43.3	15.3	3.30	Molar Root	7610 ± 20	8430 - 8380		Present Study
UCIAMS-149812	-20.7	3.5	41.8	15.0	3.26	Tooth Plate	7785 ± 25	8610 - 8475		Present Study
NB: AA26010	-21.5					3rd Molar	7908 ± 100	9015 - 8480		Present Study
NB: AA35401						3rd Molar	8015 ± 85	9125 - 8605		(80)
NB: OxA-13027						3rd Molar	8010 ± 40	9015 - 8720		(80)
NB: Mean (n=3)							8000 ± 35	9010 - 8725		
UCIAMS-119830	-20.9	4.2	42.9	15.1	3.32	Tooth	8210 ± 35	9285 - 9030	EMS 419634	Present Study
NK4: UCIAMS-149814	-19.0	7.6	40.8	14.8	3.22	Tooth Plate	8370 ± 20	9470 - 9305		Present Study
NK5: UCIAMS-149813	-19.1	6.7	44.9	16.2	3.23	Tooth Plate	8350 ± 25	9455 - 9295		Present Study
NK4/5: Mean (n=2)							8360 ± 16	9465 - 9305		

Catalogue numbers for reference specimens are in the collections of the Earth and Mineral Sciences Museum (EMS) at the Pennsylvania State University (PSU). QC; Qagnax Cave, NB; North Beach, UCI; University of California Irvine, BP; before present (1950 CE). *Range defined by 2σ

Table S2. The paleoecological and paleoenvironmental proxies sampled from the Lake Hill composite core.

		Composite core depth resolution (MCD)	
Proxy	**Thickness**	**0-860 cm**	**>860cm**
Tephra	4 cm	Every 4 cm	When visible
sedaDNA	2 cm	Every 4 cm*	Every 56 cm
Spores/Pollen	2 cm	Every 4 cm*	Every 8 cm
Macrobotanicals	2 cm	Every 4 cm	Every 8 cm
Chironomids/Diatoms/Cladocera	2 cm	Every 4 cm	Every 8 cm

Table S3. Radiocarbon dates and other age controls reported for constraining the age-depth model for the upper 740 cm of the Lake Hill sedimentary record.

PSU ID	UCIAMS ID	LacCore Section ID	Section Depth (cm)	MCD (cm)	Material Dated	Fraction Modern	$\delta^{14}C$ (‰)	^{14}C Age (BP)	Calibrated Age (BP)*
5644	128455	LAHI-LAHI13 1B-1B-1	40.5	21.5	moss gametophore, cf. *Sphagnum*	0.9726 ± 0.0017	-27.4 ± 1.7	225 ± 15	305 - 0
5645	128456	LAHI-LAHI13 1A-2L-1	62.0	181.0	moss gametophore, cf. *Sphagnum*	0.7249 ± 0.0013	-275.1 ± 1.3	2585 ± 15	2755 - 2720
5646	128457	LAHI-LAHI13 1D-2B-1	77.5	274.5	dicot leaf	0.6649 ± 0.0014	-335.1 ± 1.4	3280 ± 20	3565 - 3455
Aniakchak Tephra				*294-296*	*N/A*	*N/A*	*N/A*	*N/A*	*3595 ± 4*
5647	128458	LAHI-LAHI13 1B-6L-1	29.0	489.0	dicot leaf	0.5657 ± 0.0014	-434.3 ± 1.4	4575 ± 20	5435 - 5080
5648	128459	LAHI-LAHI13 1D-5B-1	45.0	535.0	leaf fragments	0.5120 ± 0.0012	-488.0 ± 1.2	5380 ± 20	6280 - 6030
5649	128460	LAHI-LAHI13 1B-8L-1	87.5	738.5	moss gametophore, cf. *Sphagnum*	0.2883 ± 0.0010	-711.7 ± 1.0	9990 ± 30	11615 - 11280

All results have been corrected for isotopic fractionation according to the conventions of (4). PSU; Pennsylvania State University, UCI; University of California Irvine, MCD; mean composite depth, BP; before present (1950 CE). *Range defined by 2σ.

Table S4. Normalized average major element geochemical data for the 294 cm MCD Lake Hill visible tephra.

Tephra Sample	UA #	SiO_2	TiO_2	Al_2O_3	FeO	MnO	MgO	CaO	Na_2O	K_2O	Cl	Total	H_2O diff.	n
Lake Hill, 294 cm MCD	2328/ 2654	59.38	1.33	16.35	7.68	0.22	2.79	6.13	4.45	1.56	0.12	100.00	2.57	6
		0.63	0.07	0.21	0.80	0.03	0.15	0.27	0.43	0.08	0.03	---	0.39	
	2654	71.50	0.49	15.17	2.34	0.14	0.48	1.75	4.94	3.03	0.19	100.00	1.60	72
		0.30	0.05	0.15	0.10	0.02	0.05	0.11	0.20	0.08	0.03	---	0.90	
Aniakchak CFE II reference	1602	59.02	1.40	16.49	7.76	0.22	2.77	6.25	4.40	1.59	0.12	100.00	2.34	36
		0.82	0.09	0.33	0.51	0.03	0.21	0.40	0.23	0.19	0.03	---	0.93	
		71.14	0.49	15.13	2.52	0.14	0.48	1.75	5.10	3.08	0.19	100.00	1.64	23
		0.31	0.05	0.12	0.09	0.03	0.04	0.06	0.17	0.08	0.02	---	1.12	
Lipari Obsidian	ID3506	74.06	0.08	13.09	1.56	0.07	0.02	0.72	3.99	5.19	0.32	99.02	---	60
		0.47	0.04	0.12	0.05	0.02	0.01	0.02	0.08	0.10	0.03	0.56	---	
Old Crow tephra	Oct	71.87	0.28	12.44	1.61	0.05	0.24	1.39	3.55	3.63	0.27	95.27	4.73	60
		0.91	0.04	0.19	0.06	0.02	0.02	0.04	0.25	0.13	0.03	1.16	1.16	

Averages and standard deviations for n analyzed points are shown here. Analyses have been split into distinct populations of glass where applicable. Average values for Aniakchak CFE II reference material (Zagoskin Lake, Alaska) and for secondary standards of Lipari obsidian and Old Crow tephra (81) analyzed at the same time are included for comparison.

Table S5. Sedimentary ancient DNA metadata for the Lake Hill core samples, including composite core depth, extraction method applied, sequencing statistics, and reads aligned to the African elephant, woolly mammoth, and Hoffman's two-toed sloth genomes.

Sample extract ID	Core drive and depth (cm)	MCD (cm)	Ext. method	Duplicate type	Short Read Archive accession	Raw reads (N)	P-AF reads (N)	African elephant (LoxAfr3)					Woolly mammoth					Two toed sloth (ChoHof2)				
								Pass all filters	Unique to Proboscidea	Proportion of filtered reads			Pass all filters	Unique to Proboscidea	Proportion of filtered reads			Pass all filters	Unique to Pilosa	Proportion of filtered reads		
										Replicate	Mean	1 SD			Replicate	Mean	1 SD			Replicate	Mean	1 SD
PH-EC31	N/A	N/A	2		SRR3480229	3031456	640440	3	0	4.684E-06	6.266E-06	2.237E-06	2	0	4.684E-06	6.266E-06	2.237E-06	1	0	1.561E-06	1.566E-06	5.762E-09
PH-EC32	N/A		2		SRR3480230	2999470	637115	5	0	7.848E-06			4	0	7.848E-06			1	0	1.570E-06		
PH117	1B-1B_23-25	5	3		SRR3480250	2624866	1190488	1	0	8.400E-07	1.223E-06	6.487E-07	1	0	8.400E-07	1.223E-06	6.487E-07	1	0	8.400E-07	6.087E-07	5.322E-07
PH117	1B-1B_23-25		3	3	SRR3480262	1546627	1165576	1	0	8.579E-07			1	0	8.579E-07			0	0	0.000E+00		
PH183	1B-1B_23-25		2	1	SRR3480274	1360888	1013990	2	0	1.972E-06			2	0	1.972E-06			1	0	9.862E-07		
PH116	1D-2B_67-69	265	3		SRR3480285	2815434	2292387	0	0	0.000E+00	4.089E-07	7.083E-07	0	0	0.000E+00	4.089E-07	7.083E-07	1	0	4.362E-07	1.260E-06	8.400E-07
PH116	1D-2B_67-69		3	3	SRR3480290	1592397	1419174	0	0	0.000E+00			0	0	0.000E+00			3	0	2.114E-06		
PH182	1D-2B_67-69		2	1	SRR3480291	1903215	1630223	2	0	1.227E-06			1	0	1.227E-06			2	0	1.227E-06		
PH149	1D-3B_78-80	373	2		SRR3480292	1548841	1229432	1	0	8.134E-07	8.134E-07		1	0	8.134E-07	8.134E-07		0	0	0.000E+00	0.000E+00	
PH180	1D-4B_70-72	461	2		SRR3480293	819851	685836	1	1	1.458E-06	1.458E-06		2	1	1.458E-06	1.458E-06		0	0	0.000E+00	0.000E+00	
PH178	1D-4B_74-76	465	2		SRR3480231	1550231	1293035	3	0	2.320E-06	2.320E-06		1	0	2.320E-06	2.320E-06		3	0	2.320E-06	2.320E-06	
PH179	1D-4B_78-80	469	2		SRR3480232	890555	698981	0	0	0.000E+00	0.000E+00		0	0	0.000E+00	0.000E+00		1	0	1.431E-06	1.431E-06	
PH181	1D-4B_82-84	473	2		SRR3480233	1793201	1508100	7	0	4.642E-06	4.642E-06		6	0	4.642E-06	4.642E-06		2	0	1.326E-06	1.326E-06	
PH173	1D-4B_86-88	477	2		SRR3480234	1615950	1300565	3	0	2.307E-06	1.513E-06	1.122E-06	4	0	2.307E-06	1.513E-06	1.122E-06	5	0	3.844E-06	3.722E-06	1.727E-07
PH177	1B-6L_16-18		2	2	SRR3480235	1702243	1388792	1	0	7.201E-07			2	0	7.201E-07			5	0	3.600E-06		
PH081	1B-6L_20-22	481	1		SRR3480236	1383862	1148299	5	1	4.354E-06	1.525E-06	1.952E-06	3	1	4.354E-06	1.525E-06	1.952E-06	4	0	3.483E-06	1.285E-06	1.527E-06
PH081	1B-6L_20-22		1	4	SRR3480246	2646418	2081478	0	0	0.000E+00			0	0	0.000E+00			0	0	0.000E+00		
PH155	1B-6L_20-22		2	1	SRR3480247	2283504	1915099	1	0	5.222E-07			1	0	5.222E-07			2	0	1.044E-06		
PH170	1D-4B_90-92		2	2	SRR3480248	1977174	1635223	2	0	1.223E-06			4	0	1.223E-06			1	0	6.115E-07		
PH156	1B-6L_24-26	485	2		SRR3480249	2244033	1838207	7	1	3.808E-06	3.808E-06		5	1	3.808E-06	3.808E-06		4	0	2.176E-06	2.176E-06	
PH157	1B-6L_28-30	489	2		SRR3480252	1899646	1542441	3	0	1.945E-06	1.945E-06		2	0	1.945E-06	1.945E-06		0	0	0.000E+00	0.000E+00	
PH144	1B-6L_32-34	493	2		SRR3480253	1898912	1557930	2	0	1.284E-06	1.284E-06		1	0	1.284E-06	1.284E-06		0	0	0.000E+00	0.000E+00	
PH167	1D-5B_4-6	495	2		SRR3480254	1039816	839378	0	0	0.000E+00	0.000E+00		0	0	0.000E+00	0.000E+00		0	0	0.000E+00	0.000E+00	
PH145	1B-6L_36-38	497	2		SRR3480255	1874093	1605589	6	0	3.737E-06	3.737E-06		6	0	3.737E-06	3.737E-06		1	0	6.228E-07	6.228E-07	
PH172	1D-5B_8-10	499	2		SRR3480256	1143472	904922	6	0	6.630E-06	6.630E-06		5	0	6.630E-06	6.630E-06		1	0	1.105E-06	1.105E-06	
PH142	1B-6L_40-42	501	2		SRR3480257	1712023	1375242	4	0	2.909E-06	2.909E-06		4	0	2.909E-06	2.909E-06		1	0	7.271E-07	7.271E-07	
PH143	1D-5B_12-14	503	2		SRR3480258	1899306	1507506	71	3	4.710E-05	4.710E-05		60	3	4.710E-05	4.710E-05		2	0	1.327E-06	1.327E-06	
PH168	1B-6L_44-46	505	2		SRR3480259	1545972	1129917	114	2	1.009E-04	1.009E-04		94	2	1.009E-04	1.009E-04		7	0	6.195E-06	6.195E-06	
PH148	1D-5B_16-18	507	2		SRR3480260	1506286	1272153	832	30	6.540E-04	6.540E-04		694	28	6.540E-04	6.540E-04		5	0	3.930E-06	3.930E-06	
PH169	1B-6L_48-50	509	2		SRR3480261	1962200	1555729	450	14	2.893E-04	2.893E-04		383	11	2.893E-04	2.893E-04		12	0	7.713E-06	7.713E-06	
PH150	1D-5B_20-22	511	2		SRR3480263	2280866	1861240	458	16	2.461E-04	2.461E-04		394	16	2.461E-04	2.461E-04		7	0	3.761E-06	3.761E-06	
PH175	1B-6L_52-54	513	2		SRR3480264	1904279	1532538	776	46	5.063E-04	5.063E-04		649	41	5.063E-04	5.063E-04		7	0	4.568E-06	4.568E-06	
PH152	1D-5B_24-26	515	2		SRR3480265	1952201	1557679	283	12	1.817E-04	1.817E-04		248	10	1.817E-04	1.817E-04		0	0	0.000E+00	0.000E+00	
PH171	1B-6L_56-58	517	2		SRR3480266	913972	709089	195	11	2.750E-04	2.750E-04		161	10	2.750E-04	2.750E-04		3	0	4.231E-06	4.231E-06	
PH153	1D-5B_28-30	519	2		SRR3480268	2160992	1709759	118	4	6.902E-05	6.902E-05		102	2	6.902E-05	6.902E-05		1	0	5.849E-07	5.849E-07	
PH176	1B-6L_60-62	521	2		SRR3480269	1014129	846864	229	15	2.704E-04	2.704E-04		206	17	2.704E-04	2.704E-04		3	0	3.542E-06	3.542E-06	
PH154	1D-5B_32-34	523	2		SRR3480270	2646256	2174973	1453	93	6.681E-04	6.681E-04		1236	84	6.681E-04	6.681E-04		3	0	1.379E-06	1.379E-06	
PH174	1B-6L_64-66	525	2		SRR3480271	1693131	1333499	188	5	1.410E-04	1.410E-04		155	3	1.410E-04	1.410E-04		8	0	5.999E-06	5.999E-06	
PH118	1D-5B_36-38	527	3		SRR3480272	1347732	541821	178	8	3.285E-04	1.733E-04	2.195E-04	143	5	3.285E-04	1.733E-04	2.195E-04	1	0	1.846E-06	1.771E-06	1.062E-07
PH146	1D-5B_36-38		2	1	SRR3480273	2163477	1769481	32	1	1.808E-05			31	1	1.808E-05			3	0	1.695E-06		
PH147	1D-5B_40-42	531	2		SRR3480275	1861236	1526209	257	7	1.684E-04	1.684E-04		208	6	1.684E-04	1.684E-04		4	0	2.621E-06	2.621E-06	
PH121	1D-5B_60-62	551	3		SRR3480276	1881195	432449	40	2	9.250E-05	8.415E-05	1.180E-05	29	2	9.250E-05	8.415E-05	1.180E-05	2	0	4.625E-06	3.943E-06	9.645E-07
PH186	1D-5B_60-62		2	1	SRR3480277	1473388	1226704	93	6	7.581E-05			74	4	7.581E-05			4	0	3.261E-06		
PH082	1A-6L_61-63	579	1		SRR3480278	3756988	1959968	45	1	2.296E-05	2.535E-05	3.375E-06	43	1	2.296E-05	2.535E-05	3.375E-06	11	0	5.612E-06	4.193E-06	2.008E-06
PH082	1A-6L_61-63		1	4	SRR3480279	997409	721167	20	0	2.773E-05			20	0	2.773E-05			2	0	2.773E-06		
PH083	1B-7L_46-48	599	1		SRR3480280	2736871	1975051	100	3	5.063E-05	5.279E-05	3.058E-06	76	4	5.063E-05	5.279E-05	3.058E-06	7	0	3.544E-06	2.967E-06	8.166E-07
PH083	1B-7L_46-48		1	4	SRR3480281	1048022	837030	46	1	5.496E-05			32	2	5.496E-05			2	0	2.389E-06		
PH119	1B-7L_66-68	619	3		SRR3480282	1820890	631216	268	13	4.246E-04	4.765E-04	7.339E-05	222	9	4.246E-04	4.765E-04	7.339E-05	3	0	4.753E-06	7.678E-06	4.137E-06
PH184	1B-7L_66-68		2	1	SRR3480283	1452248	1131785	598	19	5.284E-04			490	12	5.284E-04			12	0	1.060E-05		
PH151	1D-6B_37-39	679	2		SRR3480284	2420661	2093086	296	11	1.414E-04	1.414E-04		239	6	1.414E-04	1.414E-04		3	0	1.433E-06	1.433E-06	
PH120	1D-6B_77-79	719	3		SRR3480286	1892497	495780	14	2	2.824E-05	1.580E-03	2.036E-03	10	1	2.824E-05	1.580E-03	2.036E-03	1	0	2.017E-06	4.294E-06	3.674E-06
PH120	1D-6B_77-79		3	3	SRR3480287	1402382	1140268	35	1	3.069E-05			28	1	3.069E-05			1	0	8.770E-07		
PH185	1D-6B_77-79		2	1	SRR3480288	1167953	992655	4287	295	4.319E-03			3554	242	4.319E-03			9	0	9.067E-06		
PH194	1D-6B_77-79		2	1	SRR3480289	1674680	1342342	2608	178	1.943E-03			2152	160	1.943E-03			7	0	5.215E-06		
Total						98475397	70545900	14142	802				11785	686				168	0			

PH-EC31 and PH-EC32 were negative extraction controls and were not included in calculating the total number of reads passing all filters and unique hits to Proboscidea or Pilosa. Unique hits were based on BLAST analyses. Extraction method and replicate type numbers follow those listed in text S5. Pre-alignment filtered reads are merged, complexity filtered, more than 30 base pairs, and have had duplicates removed. N; frequency, SD; standard deviation, Ext; extraction, MCD; mean composite depth, P-AF; pre-alignment filtered.

Table S6. Reference genomes used for identifying mammoth ancient DNA in the Lake Hill core samples.

Species					
Common	**Scientific**	**Order**	**Higher rank**	**Assembly**	**Assembly accession**
African elephant	*Loxodonta africana*	Proboscidea	Afrotheria	LoxAfr3	GCA_000001905.1*
Woolly mammoth	*Mammuthus primigenius*	Proboscidea	Afrotheria	N/A	ERX935618*
Hoffmann's two-toed sloth	*Choloepus hoffmanni*	Pilosa	Xenarthra	ChoHof2	GCA_000164785.2
Human	*Homo sapiens*	Primates	Boreoeutheria	Hg19	GCA_000001405.1
House mouse	*Mus musculus*	Rodentia	Boreoeutheria	mm10	GCA_000001635.2
Cow	*Bos taurus*	Artiodactyla	Boreoeutheria	bosTau7	GCA_000003205.4
Horse	*Equus caballus*	Perissodactyla	Boreoeutheria	EquCab2	GCA_000002305.1

*Woolly mammoth reference mitochondrial genome (Genbank RefSeq: NC_007596.2) appended. GCA: Genbank assembly, ERX: European Nucleotide Archive.

Table S7. List of the plant taxa identified from the composite Lake Hill sedimentary record via pollen analysis.

Shrub	**Herb**
Salix	*Artemisia*
Ericaceae sp.	Asteraceae sp.
	Cyperaceae sp.
	Poaceae sp.
	Apiaceae sp.
	Stellaria
	Polemonium
	Amanranthaceae sp.
	Ambrosia
	Geranium
	Epilobium
	Campanula
	Brassicaceae sp.
	Saxifraga
	Caltha
	Ranuculus
	Rubus
	Armeria
	Valeriana
	Veronica
	Papaver
	Claytonia
	Montia
	Galium
	Primula
	Polygonaceae sp.
	Potentilla
	Gentiana
	Lupinus
	Lathyrus
	Mertensia

Table S8. Identification and composite core depth of identified plant and invertebrate macrofossil remains found in the Lake Hill core.

Plant macrofossil assignments	Item	MCD (cm)
Bryopsida, moss type 1, cf. Brachytheciaceae (cf. *Brachythecium* sp.)	gametophore	180-182
Bryopsida, moss type 2, cf. Bryidae (cf. Bryaceae, *Bryum* sp.)	gametophore	41-43; 323-331
Bryopsida, moss type 3, Polytrichaceae (cf. *Polytrichum* sp., *Polytrichastrum* sp.)	gametophore	21, 738-739
Bryopsida, moss type 4, Mniaceae (cf. *Cinclidium* sp., *Rhizomnium* sp.)	gametophore	323-325
Bryopsida, cf. moss type 5, curled leaf	loose leaves	349-351; 1268-1270
Bryopsida, moss gametophore	loose leaves, stem fragments	52-1342
Bryopsida, moss sporophyte	spore capsule	323-325
Carex sp. (Cyperaceae), sedge	achene	323-325
Juncus sp. (Juncaceae), rush	seed	1220-1222
Draba sp. (Brassicaceae), Arctic Willow Grass	seed fragment	1141-1143
Empetrum sp. (Empetriaceae), crowberry	seed coat half	389-390
Salix sp. (Salicaceae), willow	stems (wood), leaves	73-780
cf. Brassicaceae, mustards	immature silique fragment	1092-1094
cf. Fabaceae (e.g., *Lupinus sp*., lupine)	hooked trichome (?)	160-161
cf. Papaveraceae, *Corydalis* sp., few-flowered corydalis	seed/fruit	1156-1158; 1316-1326
cf. Portulacaceae, *Claytonia* sp., spring beauty	seed coat fragment	86
leaf type 2, cf. *Pyrola* sp. (Ericaceae)	skeletonized leaf	536
Crustacea	exoskeleton fragments	86-494
Trichoptera	caddisfly larvae	240-242; 323-325; 361-363
Arachnida	whole mite (n = 2)	77-79
Coleoptera	beetle elytron	77-79
unassigned spheriod with operculum		1029-1031

Supplementary References

1. Hu A, *et al.* (2010) Influence of Bering Strait flow and North Atlantic circulation on glacial sea-level changes. *Nature Geosci* 3(2):118-121.
2. Brown TA, Nelson DE, Vogel JS, & Southon JR (1988) Improved collagen extraction by modified Longin method. *Radiocarbon* 30(2):171-177.
3. Van Klinken GJ (1999) Bone collagen quality indicators for palaeodietary and radiocarbon measurements. *Journal of Archaeological Science* 26(6):687-695.
4. Stuiver M & Polach HA (1977) Discussion: Reporting of 14C data. *Radiocarbon* 19(3):355-363.
5. Ramsey CB (2009) Bayesian Analysis of Radiocarbon Dates. *Radiocarbon* 51(1):337-360.
6. Reimer PJ, *et al.* (2013) Intcal13 and Marine13 radiocarbon age calibration curves 0-50,000 years cal BP. *Radiocarbon* 55(4):1869-1887.
7. Blockley SPE, *et al.* (2005) A new and less destructive laboratory procedure for the physical separation of distal glass tephra shards from sediments. *Quaternary Science Reviews* 24(16-17):1952-1960.
8. Preece SJ, *et al.* (2011) Old Crow tephra across eastern Beringia: A single cataclysmic eruption at the close of Marine Isotope Stage 6. *Quat Sci Rev* 30(17-18):2069-2090.
9. Pearce NJ, Westgate JA, Preece SJ, Eastwood WJ, & Perkins WT (2004) Identification of Aniakchak (Alaska) tephra in Greenland ice core challenges the 1645 BC date for Minoan eruption of Santorini. . *Geochemistry, Geophysics, Geosystems* 5(3)

10. Rawlence NJ, *et al.* (2014) Using palaeoenvironmental DNA to reconstruct past environments: progress and prospects. *J. Quat. Sci.* 29(7):610-626.
11. Lydolph MC, *et al.* (2005) Beringian paleoecology inferred from permafrost-preserved fungal DNA. *Appl Environ Microb* 71(2):1012-1017.
12. Willerslev E, *et al.* (2003) Diverse plant and animal genetic records from Holocene and Pleistocene sediments. *Science* 300:791-795.
13. Giguet-Covex C, *et al.* (2014) Long livestock farming history and human landscape shaping revealed by lake sediment DNA. *Nat Commun* 5:3211.
14. D'Costa VM, *et al.* (2011) Antibiotic resistance is ancient. *Nature* 477(7365):457-461.
15. Green RE, *et al.* (2014) Three crocodilian genomes reveal ancestral patterns of evolution among archosaurs. *Science* 346(6215):1254449.
16. Fulton TL (2012) Setting up an ancient DNA laboratory. *Ancient DNA: Methods and Protocols, Methods in Molecular Biology*, eds Shapiro B & Hofreiter M (Humana Press, Springer, New York), 2012/01/13 Ed, pp 1-11.
17. Bulat SA, *et al.* (2000) Identification of a universally primed-PCR-derived sequence-characterized amplified region marker for an antagonistic strain of *Clonostachys rosea* and development of a strain-specific PCR detection assay. *Appl Environ Microbiol* 66(11):4758-4763.
18. Haile J (2012) Ancient DNA extraction from soils and sediments. *Ancient DNA: Methods and Protocols, Methods in Molecular Biology*, eds Shapiro B & Hofreiter M (Humana Press, Springer, New York), Vol 840, pp 57-63.
19. Wales N, Andersen K, Cappellini E, Avila-Arcos MC, & Gilbert MT (2014) Optimization of DNA recovery and amplification from non-carbonized archaeobotanical remains. *PLoS One* 9(1):e86827.

20. Barnes I, *et al.* (2007) Genetic structure and extinction of the woolly mammoth, *Mammuthus primigenius*. *Current Biology* 17(12):1072-1075.
21. Palkopoulou E, *et al.* (2013) Holarctic genetic structure and range dynamics in the woolly mammoth. *Proc Biol Sci* 280(1770):20131910.
22. Taylor PG (1996) Reproducibility of ancient DNA sequences from extinct pleistocene fauna. *Mol Biol Evol* 13(1):283-285.
23. Haile J, *et al.* (2009) Ancient DNA reveals late survival of mammoth and horse in interior Alaska. *Proceedings of the National Academy of Sciences* 106(52):22352-22357.
24. Boessenkool S, *et al.* (2012) Blocking human contaminant DNA during PCR allows amplification of rare mammal species from sedimentary ancient DNA. *Mol Ecol* 21(8):1806-1815.
25. Meyer M & Kircher M (2010) Illumina sequencing library preparation for highly multiplexed target capture and sequencing. *Cold Spring Harbor Protocols* 2010(6):pdb prot5448.
26. Heintzman PD, *et al.* (2015) Genomic data from extinct North American *Camelops* revise camel evolutionary history. *Mol Biol Evol* 32(9):2433-2440.
27. Morgulis A, Gertz EM, Schaffer AA, & Agarwala R (2006) A fast and symmetric DUST implementation to mask low-complexity DNA sequences. *J Comput Biol* 13(5):1028-1040.
28. Schmieder R & Edwards R (2011) Quality control and preprocessing of metagenomic datasets. *Bioinformatics* 27(6):863-864.
29. Palkopoulou E, *et al.* (2015) Complete genomes reveal signatures of demographic and genetic declines in the woolly mammoth. *Curr Biol* 25(10):1395-1400.
30. Li H & Durbin R (2009) Fast and accurate short read alignment with Burrows-Wheeler transform. *Bioinformatics* 25(14):1754-1760.

31. Schubert M, *et al.* (2012) Improving ancient DNA read mapping against modern reference genomes. *Bmc Genomics* 13:178.
32. Li H, *et al.* (2009) The Sequence Alignment/Map format and SAMtools. *Bioinformatics* 25(16):2078-2079.
33. dos Reis M, *et al.* (2012) Phylogenomic datasets provide both precision and accuracy in estimating the timescale of placental mammal phylogeny. *Proc Biol Sci* 279(1742):3491-3500.
34. McDonald HG, Harington CR, & de Iuliis G (2000) The Ground Sloth *Megalonyx* from Pleistocene Deposits of the Old Crow Basin, Yukon, Canada. *Arctic* 53(3):213-220.
35. Veltre DW, Yesner DR, Crossen KJ, Graham RW, & Coltrain JB (2008) Patterns of faunal extinction and paleoclimatic change from mid-Holocene mammoth and polar bear remains, Pribilof Islands, Alaska. *Quaternary Research* 70(1):40-50.
36. Jonsson H, Ginolhac A, Schubert M, Johnson PL, & Orlando L (2013) mapDamage2.0: fast approximate Bayesian estimates of ancient DNA damage parameters. *Bioinformatics* 29(13):1682-1684.
37. Prüfer K & Meyer M (2015) Comment on "Late Pleistocene human skeleton and mtDNA link Paleoamericans and modern Native Americans". *Science* 347(6224):835-835.
38. Dabney J, Meyer M, & Paabo S (2013) Ancient DNA damage. *Cold Spring Harbor Perspectives in Biology* 5:1-7.
39. Faegri K, Kaland PE, & Krzywinski K (1989) *Textbook of Pollen Analysis* (John Wiley & Sons Ltd.).
40. Colinvaux P (1981) Historical ecology in Beringia: The south land bridge coast at St. Paul Island. *Quaternary Research* 16(1):18-36.

41. Aiken SG, *et al.* (2007) *Flora of the Canadian Arctic Archipelago: Descriptions, Illustrations, Identification, and Information Retrieval.* (NRC Research Press, National Research Council of Canada).
42. Hultén E (1960) *Flora of the Aleutian Islands and Westernmost Alaska Peninsula with Notes on the Flora of Commander Islands.* (J. Cramer, New York) Second Ed.
43. Hultén E (1968) *Flora of Alaska and Neighboring Territories: a Manual of the Vascular Plants.* (Stanford University Press, Stanford, CA).
44. Martin AC & Barkley WD (1961) *Seed Identification Manual.* (Univeristy of California Press, Berkeley).
45. Metcalf CR (1960) *Anatomy of the Monocotyledons* (Oxford Clarendon Press, Oxford, UK).
46. Metcalf CR (1971) *Anatomy of the Monocotyledons* (Oxford Clarendon Press, Oxford, UK).
47. Panshin AJ & de Zeeuw C (1980) *Textbook of Wood Technology: Structure, Identification, Uses, and Properties of the Commerical Woods of the United States and Canada* (McGraw-Hill Book Company, New York) Fourth Ed p 705.
48. InsideWood (2015) InsideWood. 2004-onwards.).
49. Wheeler EA, Pearson RG, LaPasha CA, Zack T, & Hatley W (1986) *Computer-Aided Wood Identification* (North Carolina State University, Raleigh).
50. Goffinet B & Shaw AJ eds (2009) *Bryophyte Biology* (Cambridge University Press, UK), Second Ed.
51. Smith GM (1955) *Cryptogamic Botany: Bryophytes and Pteridophytes* (McGraw Hill, New York).
52. CNABH (2015) Consortium of North American Bryophyte Herbaria.).

53. Ellis S (2015) Introduction to Bryophytes: The Public Face of Biology 321, University of British Columbia, Vancouver, Canada. Vancouver).
54. Stotler RE & Crandall-Stotler BJ (2015) Bryophytes. (Department of Plant Biology, Southern Illinois University, Carbondale).
55. Barber KE (1981) *Peat Stratigraphy and Climatic Change: a Palaeoecological Test of the Theory of Cyclic Peat Bog Regeneration* (Balkema, Rotterdam).
56. Barber KE & Langdon PG (2001) Peat stratigraphy and climate change. *Handbook of Archaeological Sciences*, eds Brothwell DR & Pollard AM (Wiley, Chichester), pp 155-166.
57. Janssens JA (1983) A quantitative method for stratigraphic analysis of bryophytes in Holocene peat. *Journal of Ecology* 71(1):189-196.
58. Battarbee RW, *et al.* (2001) Diatoms. *Tracking environmental change using lake sediments, Vol. 3: Terrestrial, Algal and Siliceous Indicators*, eds Smol JP, Birks HJB, & Last WM (Kluwer Academic Publishers, Dordrecht), pp 155-202.
59. Antoniades D, Hamilton PB, Douglas MSV, & Smol JP (2008) Diatoms of North America: The freshwater floras of Prince Patrick, Ellef Ringnes, and Northern Ellesmere Islands from the Canadian Arctic Archipelago. *Iconographica Diatomologica* 17:1-649.
60. Cumming BF, Wilson SE, Hall RI, & Smol JP (1995) *Diatoms from British Columbia (Canada) lakes and their relationship to salinity, nutrients and other limnological variables* (Cramer, J., Berlin) p 207.
61. Fallu M-A, Allaire N, & Pienitz R (2000) *Freshwater diatoms from northern Québec and Labrador (Canada): species–environment relationships in lakes of boreal forest, forest–tundra and tundra regions* (Cramer, J., Berlin) p 200.

62. Korhola A & Rautio M (2001) Cladocera and other branchiopod crustaceans. *Tracking environmental change using lake sediments, Vol. 4: Zoological Indicators*, eds Smol JP, Birks HJB, & Last WM (Kluwer Academic Publishers, Dordrecht), pp 5-41.
63. Alonso M (1996) Crustacea Branchiopoda. *Fauna Iberica*, (Museo Nacional de Ciencias Naturales, CSIC, Madrid), Vol 7.
64. Flössner D (1972) Krebstiere, Crustacea: Kiemen- und Blattfüsser, Branchiopoda, Fischlduse, Branchiura. *Die Tierwelt Deutschlands*, (Fisher, Jena), Vol 60, p 501.
65. Frey DG (1958) The late-glacial cladoceran fauna of a small lake. *Arch. Hydrobiol.* 54:209-275.
66. Smirnov NN (1971) Chydoridae of the world fauna. Fauna USSR. *Crustacea 1 No. 2*, Leningrad), Vol 101, p 529.
67. Blaauw M & Christen JA (2011) Flexible paleoclimate age-depth models using an autoregressive gamma process. *Bayesian Analysis* 6:1-18.
68. Erdman C & Emerson JW (2007) bcp: An R Package for Performing a Bayesian Analysis of Change Point Problems. *Journal of Statistical Software* 23:1-13.
69. Gregory-Eaves I, Smol JP, Finney BP, & Edwards ME (1999) Diatom-based transfer functions for inferring past climatic and environmental changes in Alaska, U.S.A. *Arctic, Antarctic and Alpine Research* 31(4):353-365.
70. Fritz SC, Juggins S, Battarbee RW, & Engstrom DR (1991) Reconstruction of past changes in salinity and cliamte using a diatom-based transfer function. *Nature* 352:706-708.
71. Wilson SE, Cumming BF, & Smol JP (1994) Assessing the reliability of salinity inference models from diatom assemblages: an examination of a 219-lake data set from western North America. *Canadian Journal of Fisheries and Aquatic Sciences* 53:1580-1594.

72. Bos DG, Cumming BF, & Smol JP (1999) Cladocera and Anostraca from the Interior Plateau of British Columbia Canada, as paleolimnological indicators of salinity and lake level. *Hydrobiologia* 392:129–141.
73. Thienpont JR, *et al.* (2013) Exploratory hydrocarbon drilling impacts to Arctic lake ecosystems. *PLoS One* http://dx.plos.org/10.1371/journal.pone.0078875
74. Chengalath R (1982) A faunistic and ecological survey of littoral Cladocera of Canada. *Canadian Journal of Zoology* 60:2668–2682.
75. Deasley K, *et al.* (2012) Investigating the response of Cladocera to a major saltwater intrusion event in an Arctic lake from the outer Mackenzie Delta (NT, Canada). *Journal of Paleolimnology* 48:287–296.
76. Wooller MJ, *et al.* (2004) Quantitative paleotemperature estimates from delta O-18 of chironomid head capsules preserved in arctic lake sediments. *Journal of Paleolimnology* 31(3):267-274.
77. Wooller MJ, *et al.* (2012) Reconstruction of past methane availability in an Arctic Alaska wetland indicates climate influenced methane release during the past similar to 12,000 years. *Journal of Paleolimnology* 48(1):27-42.
78. Wooller MJ, *et al.* (2012) An ~11,200 year paleolimnological perspective for emerging archaeological findings at Quartz Lake, Alaska. *Journal of Paleolimnology* 48(1):83-99.
79. Grover MA & Tedor R (2006) A Mid-Holocene Mammoth Tusk from St. Paul Island. in *The annual meeting of the Alaska Anthropological Association*Kodiak).
80. Guthrie RD (2004) Radiocarbon evidence of mid-Holocene mammoths stranded on an Alaskan Bering Sea island. *Nature* 429(6993):746-749.

81. Kuehn SC, Froese DG, Shane PAR, & Participants II (2011) The INTAV intercomparison of electron-beam microanalysis of glass by tephrochronology laboratories: Results and recommendations. *Quaternary International* 246(1-2):19-47.